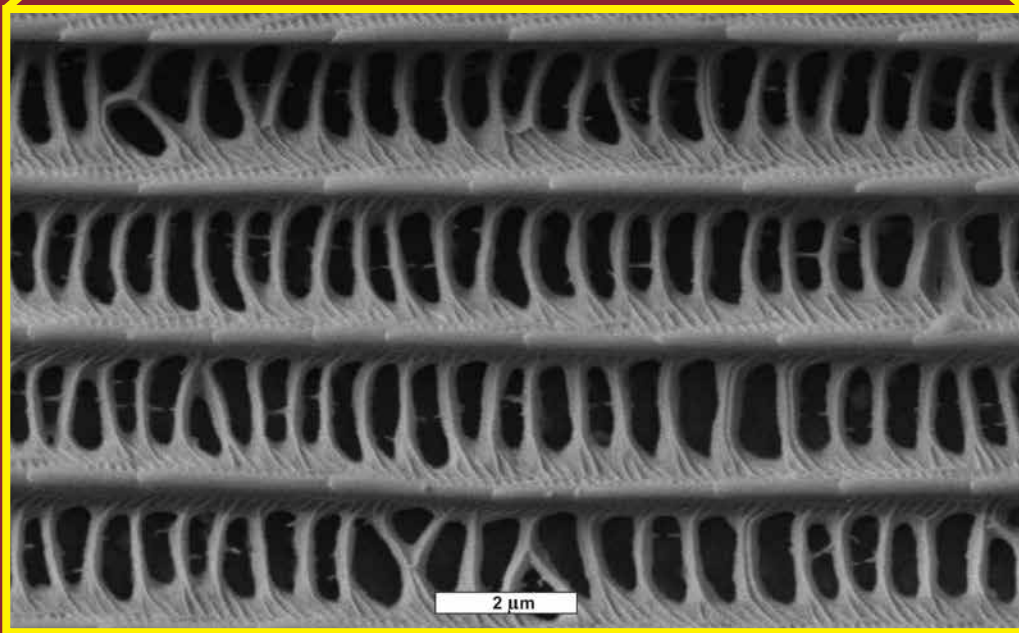
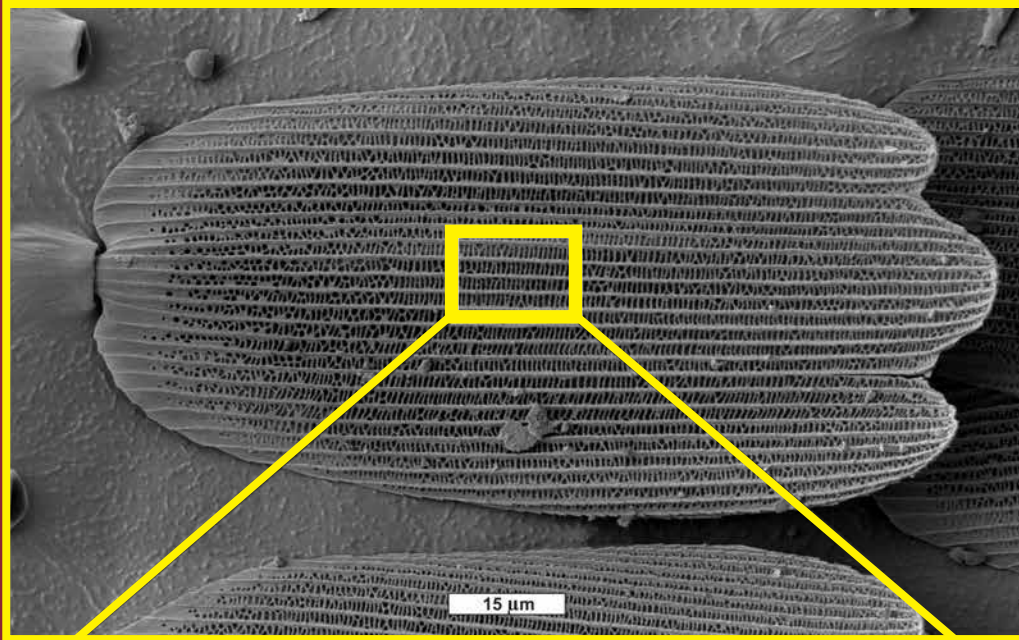


Texas Journal of Microscopy

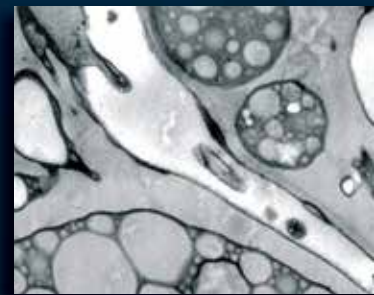
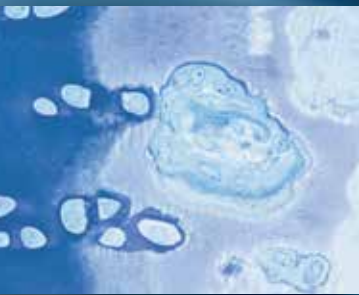


Volume 49
Number 1, 2018
ISSN 1554-0820

Visit our website at www.texasmicroscopy.org

DiATOME *diamond knives*

**the highest quality...
the most precise sectioning...
incomparable durability**



building on 40 years of innovation

*ultra 45° • cryo • histo • ultra 35°
histo jumbo • STATIC LINE II • cryo immuno
ultra sonic • ultra AFM & cryo AFM*

NEW!... trimtool 20 and trimtool 45
*Finally, one trimming tool for all of your trimming
needs, be it at room or cryo temperatures.*

DiATOME U.S.

P.O. Box 550 • 1560 Industry Rd. • Hatfield, Pa 19440
Tel: (215) 412-8390 • Fax: (215) 412-8450
email: sgkcck@aol.com • stacie@ems-secure.com
www.emsdiasum.com

TSM OFFICERS 2017-2018

President

BERND ZECHMANN
Center for Microscopy and Imaging
Baylor University
One Bear Place #97046 • Waco, Texas 76798-7046
(254) 710-2322 • FAX (254) 710-2405
Bernd_Zechmann@baylor.edu

Past-President

LAURA HANSON
Department of Biology
Texas Woman's University • Denton, Texas 76204-5799
(940) 898-2472 • FAX (940) 898-2354 • lhanson@twu.edu

President-Elect

VACANT

Secretary

CATALINA I. PISLARIU
Department of Biology
Texas Woman's University • Denton, Texas 76204-5799
(940) 898-4611 • FAX (940) 898-2354 • cpislariu@twu.edu

Secretary-elect

VACANT

Treasurer

DAVID GARRETT
Dept. of Materials Science and Engineering
University of North Texas • Denton, Texas 76203-5017
(940) 369-8836 • dgarrett@unt.edu

Treasurer-elect

VACANT

Program Chairman

SANDRA WESTMORELAND
Department of Biology
Texas Woman's University • Denton, Texas 76204-5799
(940) 898-2560 • FAX (940) 898-2382
swestmoreland@twu.edu

Program Chairman-elect

AMY JO M. HAMMETT
Department of Biology
Texas Woman's University • Denton, TX 76204-5799
(940) 898-2397 • FAX (940) 898-2382
AHammett1@twu.edu

APPOINTED OFFICERS

Corporate Member Representative

JAMES LONG
5794 W. Las Positas Blvd. • Pleasanton, CA 94588
(512) 657-0898 • FAX (925) 463-0504 • jlong@gatan.com

Student Representative

AUDREY HOWARD
Dept. of Life, Earth, and Environmental Sciences
West Texas A&M University • Canyon, Texas 79015
(806) 632-9759 • adhoward3@buffs.wtamu.edu

Journal Editors

CAMELIA MAIER
Department of Biology
Texas Woman's University • Denton, Texas 76204-5799
(940) 898-2358 • FAX (940) 898-2354 • cmaier@twu.edu

CATALINA I. PISLARIU

Department of Biology
Texas Woman's University • Denton, Texas 76204-5799
(940) 898-4611 • FAX (940) 898-2354 • cpislariu@twu.edu

Webmaster

BERND ZECHMANN
Center for Microscopy and Imaging
Baylor University
One Bear Place #97046 • Waco, Texas 76798-7046
(254) 710-2322 • FAX (254) 710-2405
Bernd_Zechmann@baylor.edu

Facebook Master

NABARUN GHOSH
Dept. of Life, Earth, and Environmental Sciences
West Texas A&M University • Canyon, Texas 79015
(806) 651-2571 • FAX (806) 651-2928
nghosh@mail.wtamu.edu

Contents



TEXAS JOURNAL OF MICROSCOPY

VOLUME 48, NUMBER 1, 2018

ISSN 1554-0820

Editor

Camelia Maier, PhD
Department of Biology, Texas Woman's University, Denton, TX 76204

Co-Editor

Catalina I. Pislariu, PhD
Department of Biology, Texas Woman's University, Denton, TX 76204

Official Journal of the Texas Society for Microscopy

"TSM - Embracing all forms of Microscopy"

www.texasmicroscopy.org

President's Message	5
Invited Presentations for the 53rd TSM Meeting.....	6
Spring 2018 Meeting Abstracts.....	8
Beam Deceleration Improves Image Quality of Butterfly Wing Scales in the Scanning Electron Microscope.....	26
Corporate Members	20

Advertiser's Index:

Diatome	2
Gatan	4
Thermo Fisher Scientific.....	7
Tousimis.....	28
Micro Star Technologies	31
Electron Microscopy Sciences	32

ON THE COVER

Scanning electron micrographs of a butterfly wing scale (*Agraulis* sp.) taken under high vacuum conditions with 5kV beam acceleration, 2kV beam deceleration, resulting in a final beam energy on the surface of the sample of 3kV. See more details in the article entitled 'Beam deceleration improves image quality of butterfly wing scales in the scanning electron microscope' by B. Zechmann, Baylor University, Waco, TX 76798-7046 starting on page 26 of this journal issue.

Introducing K3 and Rio

The Future of Imaging is Here

Gatan proudly introduces the new K3 and Rio cameras for transmission electron microscopy. All Gatan cameras now feature custom designed CMOS sensors that are exclusive to Gatan. With these best-in-class cameras, Gatan again sets new benchmarks in high-performance imaging in electron microscopy.

K3

- 24 megapixels, 1500 fps
- Single electron counting direct detection camera
- Unrivaled performance in low-dose applications
- Optional inline GPU-based motion correction



OneView

- 16 megapixels, 25 fps
- Highest resolution scintillator camera
- Optimized for aberration-corrected TEM up to 300 kV
- Optional *in-situ* data capture



Rio

- 9 – 16 megapixels, 15 – 20 fps
- Exclusive Gpixel CMOS sensors
- Optimized for 120 – 200 kV TEM
- Optional *in-situ* data capture



President's Message

It has been a very busy year for the Texas Society for Microscopy (TSM) and with the help of the Executive Council we have accomplished a lot. In spring 2017 we launched a platform on our website that can be used now to register for our annual meeting and apply for membership. We also revised the By-laws of our Society, which are up for approval at our next business meeting in Denton. In August 2017, I represented the TSM at the M&M meeting in St. Louis and met affiliates of other microscopy societies across the United States. Most recently, we have begun to digitize and archive past issues of the Texas Journal of Microscopy and Society's documents. With the support of student helpers at Baylor University in Waco, we have scanned over 80 issues and thousands of document pages from the 1960s up to 2000s. Past issues of the society journal are available as open access for all interested audience on our webpage, www.texasmicroscopy.org.

Sandra Westmoreland, our 2017-2018 Program Chair, has been working hard to organize the 53rd annual meeting in Denton. She has done a great job and I want to express my thank for her efforts. I also want to thank Nikon for organizing a magnificent workshop. This year's invited speakers are two well-known scientists, Daniela Nicastro of the Departments of Cell Biology and Biophysics at the UT Southwestern Medical Center in Dallas, a specialist in cryo-electron microscopy, and Robert M. Wallace of the Department of Materials Science and Engineering at the UT Dallas, a specialist in high-resolution microscopy of 2D materials (see the summaries of their presentations on the next page). My special thanks go out to our journal editor, Camelia Maier, for all the time and effort she spent in preparing, designing, and publishing the 2018 issue of our journal.

We are also planning for the future. Amy Jo, our Program Chair-Elect, has already started to organize our 2019 annual meeting, which will be held in San Antonio, in connection with the University of Texas there. Our host and local organizer is Josefina Arellano-Jimenez, director of the

Kleberg Advanced Microscopy Center at UT. Taking into account Amy Jo's and Josefina's enthusiasm for the job and great organization skills, I am very confident that the 54th annual meeting will turn out to be a great meeting and hope to see all TSM members in the beautiful San Antonio in 2019.

Our Society is in very good financial health, according to our treasurer's reports. I want to take this opportunity to thank David Garrett for his work as the Treasurer for so many years. Also, I want to thank James Long for representing the corporate members, and Aubrey Howard for representing our student members in the Executive Council. I am grateful for Nabarun Ghosh's support as the Society's Facebook manager, for his eagerness and promptness in keeping that page up to date, and for Catalina Pislariu's essential support as the Society's Secretary. Many thanks also go to all our corporate members, regular members, and student members for supporting the TSM with their membership and participation at our annual meeting.

Finally, I want to mention that it has been very exciting for me to hear that the Nobel Prize for Chemistry in 2017 has been awarded to three scientists that have developed methods to image biomolecules with cryo-electron microscopy. The TSM congratulates the recipients. This shows that microscopy is more important than ever in our research and should come as a great motivation for all of us who use, love, and teach microscopy. It has been an honor and pleasure serving as the 2017-2018 TSM President and sharing my enthusiasm for microscopy with our members.

Bernd Zechmann
TSM President, 2017-2018

TEXAS SOCIETY FOR MICROSCOPY'S 53RD ANNUAL MEETING

INVITED PRESENTATIONS

PROBING THE MOLECULAR ORGANIZATION OF CELLS AND ORGANELLES USING CRYO-ELECTRON MICROSCOPY

DANIELA NICASTRO

**Departments of Cell Biology and Biophysics, University of Texas Southwestern Medical Center,
Dallas, Texas 75390**

Rapid freezing of cells can provide outstanding structure preservation and time resolution of dynamic cellular processes. Electron tomography of rapidly frozen specimens (cryo-ET) is a powerful technique for imaging biological structures in their native state and in an unperturbed cellular environment. We integrate high resolution imaging by either cryo-ET and sub-tomogram averaging or TYGRESS (Tomography-Guided 3D Reconstruction of Subcellular Structures), with comparative genetics, biochemical methods and EM-visible labeling to deconstruct the in situ 3D structure and functional organization of macromolecular complexes. Among different model systems, we use cilia and flagella to advance techniques and approaches for high-resolution imaging of complex cellular structures. Cilia and flagella are conserved and ubiquitous eukaryotic organelles that are composed of more than 600 different proteins and have important biological roles in motility and sensation. Defects in their assembly or function cause severe human diseases. Our cryo-ET studies visualize the three-dimensional structures of intact wild-type and mutant flagella, and dissect the organization of key macromolecular complexes in different functional states. Such information can provide detailed insights into the structural basis and ultimately the function of many cellular processes.

HIGH-RESOLUTION MICROSCOPY OF 2D MATERIALS AND THE IMPLICATIONS FOR FUTURE DEVICE TECHNOLOGIES

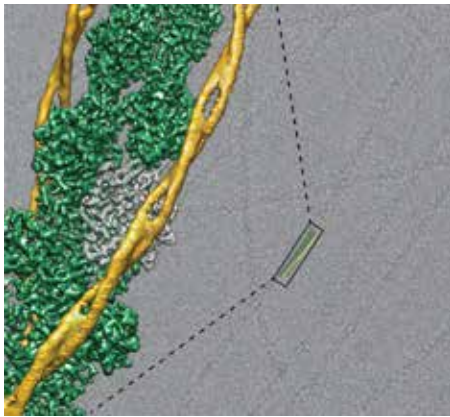
ROBERT M. WALLACE

**Professor and Erik Jonsson Distinguished Chair
Department of Materials Science and Engineering, The University of Texas at Dallas**

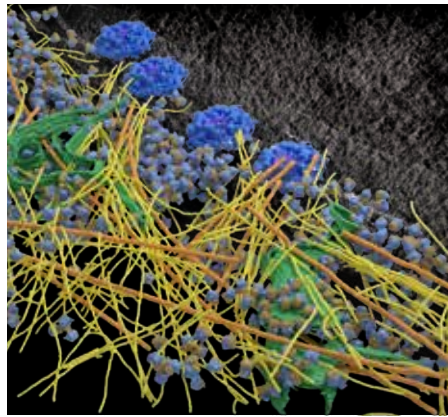
The size reduction and economics of integrated circuits, captured since the 1960's in the form of Moore's Law, continues to be challenged. Challenges include addressing aspects associated with truly atomic dimensions, while the cost of manufacturing is increasing such that only 3 or 4 companies can afford leading edge capabilities. To address some of the materials physical limitations, "2D materials" such as graphene, phosphorene, h-BN, and transition metal dichalcogenides have captured the imagination of the electronics research community for advanced applications in nanoelectronics and optoelectronics. Among 2D materials "beyond graphene," some exhibit semiconducting behavior, such as transition-metal dichalcogenides (TMDs), and present useful bandgap properties for applications even at the single atomic layer level. Examples include "MX₂", where M = Mo, W, Sn, Hf, Zr and X = S, Se and Te. The ideal materials properties have much appeal, but the reality of defects, impurities, and materials integration constraints will surely compromise the intrinsic performance of such device technologies. This talk will present a sample of our recent work employing high-resolution microscopy (STEM and STM) examining defects, impurities, functionalization, as well as the implications for process integration for electronic and optoelectronic applications (McDonnell and Wallace, 2016).

Discover Life-changing Answers Faster

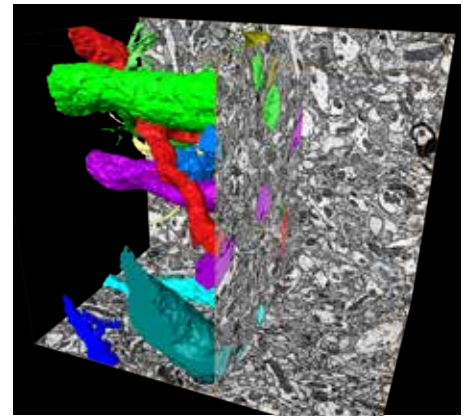
Three workflows to reveal the ultimate structural details



Courtesy of Julian von der Ecken and Prof. Dr. Stefan Raunser, Max Planck Institute of Molecular Physiology, Dortmund, Germany.



Courtesy of Dr. J. Mahamid, Max Planck Institute of Biochemistry, Martinsried, Germany.



Courtesy of Dr. P. Laserstein, Max Planck Institute, Brain Research, Germany.

Single Particle Analysis

- Total solution for 3D structural determination from sample preparation to 3D data analysis
- Most automated cryo-EM platforms for maximum throughput and reduced cost per structure
- Thermo Scientific™ Falcon 3EC™ direct electron detector, Phase Plate and EPU™ software enhance Krios™, Talos Arctica™, and Glacios™ cryo-TEM performance through data quality and ease-of-use
- Proven cryo-EM technology is the most selected solution in global top-level labs

Cryo-Tomography

- Nanometer-scale 3D models of biological structures in their native, cellular context
- Open windows into cells with dedicated cryo-TEM lamella preparation system, the Thermo Scientific Aquilos™ cryo-FIB.
- Produce cryo-lamellas for cryo-tomography without cutting artifacts

Large Volume Analysis

- Large volume data acquisition with DualBeam™ systems, serial block face imaging or array tomography
- Three applications for the region of interest
- Total workflow solution from one provider

Find out more at [thermofisher.com/FEI](https://www.thermofisher.com/FEI)

ThermoFisher
SCIENTIFIC

Abstracts

BIOLOGICAL SCIENCES Spring 2018

AN HDAC8-H1.3 PROTEIN COMPLEX IS ASSOCIATED WITH TRANS-GOLGI VESICLES AND LATE ENDOSOMES IN THE BREAST ADENOCARCINOMA MCF-7 CELLS. THU DOAN, RHIANNON WOLD GONZALEZ, CARRIE WILKS, AND MICHAEL BERGEL, Texas Woman's University, Department of Biology, Denton, TX 76204-5799

Histone deacetylase 8 (HDAC8) and linker histone subtype H1.3 are two proteins associated with chromatin compaction and transcriptional repression. In a screen for complexes between HDACs and H1 proteins, we found that HDAC8 and H1.3 formed a complex. However, the HDAC8-H1.3 complex was detected in an unexpected cellular location—cycling vesicles in the cytoplasm of MCF7 breast adenocarcinoma cells. Co-localization with Rab7 narrowed down the HDAC8-H1.3 complex localization to trans-Golgi vesicles and late endosomes. Mass spectrometry suggested that the HDAC8-H1.3 complex is associated with the vesicular proteins COPA, Sec23A, Sec23B, Sec22B, and clathrin heavy chain 1. Through co-immunoprecipitation followed by Western blotting, we validated the binding of clathrin heavy chain 1 to the HDAC8-H1.3 complex. To further corroborate the association of clathrin heavy chain 1 with the HDAC8-H1.3 complex, immunofluorescence staining followed by confocal microscopy will be testing for co-localization. To summarize, our research describes a novel HDAC8-H1.3 protein complex associated with clathrin heavy chain 1 and localized to trans-Golgi vesicles and late endosomes, an atypical cellular location for chromatin binding proteins. Our future goal is to determine the functional role of this complex in vesicular trafficking, which is an important component of many biological processes, such as endocrine secretion and neurotransmission.

AN EVOLUTIONARY MODEL OF HETEROTOPIC OSSIFICATION IN HUMANS – THE AMERICAN ALLIGATOR (*ALLIGATOR MISSISSIPPIENSIS*). BENJAMIN DUBANSKY¹ and BROOKE DUBANSKY², ¹Department of Biological Sciences, Developmental Integrative Biology Research Cluster, University of North Texas, Denton, Texas, 76203, ²Department of Medical Laboratory Sciences & Public Health, Tarleton State University, Fort Worth, TX 76104

Heterotopic ossification (HO) occurs in humans when bone forms in soft tissues. These bones are qualitatively

normal and can form following traumatic tissue injury, as a result of several underlying diseases, and can be idiopathic. Unfortunately, there are no viable treatment options for HO since removal of the tissue often exacerbates the formation of additional bone, and few laboratory models are available to study HO. Evolutionary model organisms (EMOs) retain adaptations that either represent or reflect the pathogenesis of human disease. EMOs can be powerful representations of natural processes since these animals can be studied without laboratory manipulation and retain polygenic complexity. In the American alligator (*Alligator mississippiensis*), dermal ectopic bones called osteoderms form within mature, differentiated dermis of dorsal scales (Fig. 1). It was previously assumed that osteoderms formed *via* non-cell mediated direct osseous metaplasia, although there was no physiological mechanistic basis for this assumption. Here, an extensive histological evaluation was completed using classical, modified and immunohistochemical methodologies to illustrate the first detailed description of alligator osteoderm development. The results showed definitive evidence that osteoderms form through cell-mediated, intramembranous ossification, not direct osseous metaplasia. These data also depict how an endothelial-to-mesenchymal transition occurs to generate bone precursors. Importantly, this work also shows that the mechanism of ossification within the alligator scale bears striking similarities with the proposed mechanisms of several HO forms. As such, these data suggest that the American alligator is a useful EMO for studying HO in human disease.

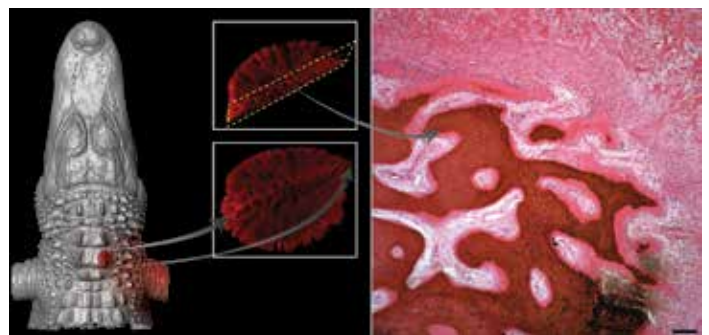


Fig. 1. Developmental progression of osteoderm formation. Alligator scales from the nuchal crest were excised and sectioned along a sagittal plane at several stages of early development (left). Development of the osteoderm was described *via* an extensive histological assessment (right), which detailed the mechanism of osteoderm development from the initiation of bone formation from a cellular condensation within a fibrotic area, through several osteogenic stages, to eventually form intramembranous bone with a fully-calcified matrix. Scale bar = 40 μ .

DETERMINING HOW TGF- β IS TRAFFICKED AND SECRETED IN *C. ELEGANS*. GEETHANJALI RAVINDRANATHAN, LIONEL FAURE, and TINA L. GUMIENNY*, Department of Biology, Texas Woman's University, Denton, Texas 76204-5799

Transforming growth factor-beta (TGF- β) comprises a conserved family of secreted cell signaling proteins responsible for regulating numerous cellular processes. Disruption of TGF- β signaling results in developmental defects and cancer in mammals. In the nematode *Caenorhabditis elegans*, one TGF- β superfamily member is DBL-1. To identify potential targets that affect DBL-1 signaling, an RNAi screen was performed that identified candidates that may be involved in neuronal trafficking and secretion of DBL-1 from the sending cell, a process that is not well understood for any TGF- β signaling protein. Specific aims of this research project are to determine if 1) the candidate genes and *dbl-1* interact genetically and 2) their proteins co-localize. Genetic and confocal microscopy analyses of transgenic *C. elegans* strains expressing functional, fluorescently tagged DBL-1 and candidate regulators provide insight into how cells regulate the message they send. Candidates include the small GTPases RAP-1 and UNC-108, caveolin CAV-1, and dynamin DYN-1. Genetic interaction and co-localization studies with synaptic vesicle acetylcholine transporter UNC-17 suggests that this complex also affects DBL-1 within the secreting neurons. While RNAi of the retrograde trafficking and autophagy gene *bec-1* reduces GFP-tagged DBL-1, tagged, functional BEC-1 does not co-localize with DBL-1, suggesting an indirect involvement in DBL-1 trafficking.

SYNTHESIS, CHARACTERIZATION, AND PRESERVATION OF SUBMICRON-SIZED LIPOSOMES AS CARRIERS FOR DRUG DELIVERY. H. LUJAN¹, B. ZECHMANN², and C. M. SAYES¹ ¹Environmental Science, Baylor University, Waco, Texas, ²Center for Microscopy and Imaging, Baylor University, Waco, Texas

In recent years, liposomes synthesized in the submicron-size range have been shown to facilitate drug delivery into cancer cells. These ultra-small liposomes are ideal candidates as drug delivery carriers (DDC) because of their bioavailability and biocompatibility. One major challenge, however, when using liposomes as DDCs, is the lack of controllable manufacturing conditions that often result in little control of the critical quality attributes (CQAs) needed for successful drug delivery. Furthermore, the shelf life of such materials is very short (<2 weeks) and therefore they are not suited for distribution. This study is designed to understand the exact CQAs of liposomes that dictate their size heterogeneity and instability so that those parameters could be fine-tuned. To accomplish this goal, liposomes have been synthesized and characterized in wetted and dried states (e.g. air-dried, lyophilized, and critical point dried).

Using light, fluorescence, and electron microscopy techniques, the size, size distribution, morphology, and encapsulation efficiency of the liposomes were analyzed. Other techniques such as fluorescence spectroscopy and light scattering corroborated microscopy results. Specifically, light microscopy and transmission electron microscopy measured size and distribution, scanning electron microscopy determined surface morphologies, and fluorescence microscopy measured encapsulation efficiency.

Our data suggest that liposomes in the size range of 20-100 μm and dried using lyophilization produced the most stable samples with a shelf life of more than 1 month in storage. The ultra-small liposomes in the size range of 50-200 nm had the most homogeneous size population per synthesis and after extrusion to remove the larger artifacts. These results serve as a platform for employing future routine liposome characterization techniques for assessing CQAs. The protocols used are valuable for sample preparation using microscopy techniques. With the increase in quality control for liposome synthesis, DDCs may become accessible for more drug delivery applications.

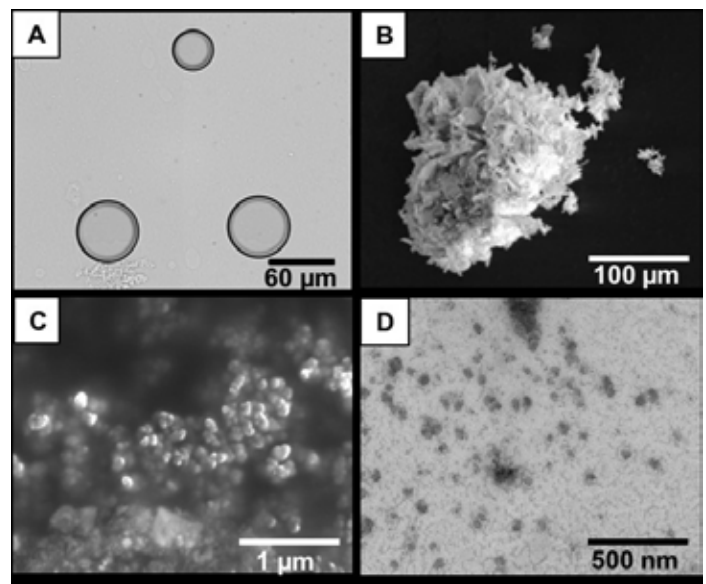


Fig. 1. Representative micrograph of liposomes. (A) Light microscopy image of air-dried micron-sized liposomes. (B) SEM image of lyophilized micron-sized liposome. (C) SEM image of ultra-small air-dried liposomes. (D) TEM image of ultra-small lyophilized liposomes. All liposomes imaged via electron microscopy were first fixed with 2% osmium tetroxide for 10 min.



MICROSCOPIC AND QUANTITATIVE ASSESSMENT OF AEROSOL DECAY AND REDUCTION OF AEROALLERGENS USING AHPCO AND BI-POLAR UNITS. AUBREY HOWARD¹, CHANDINI REVANNA², NELOFAR SHERALI¹, JON BENNERT³, JEFF BENNERT³, NABARUN GHOSH¹, NARUKI HIRANUMA¹, JIM ROGERS¹, JAY VITALE⁴ and CONSTANTINE SAADEH⁵,
¹Department of Life, Earth and Environmental Sciences, West Texas A&M University, Canyon, Texas 79015, ²Department of Environmental Toxicology, Texas Tech University, Lubbock, Texas 79416, ³Air Oasis, Amarillo, Texas 79118, ⁴Air for Life, London, UK, ⁵Allergy ARTS, Amarillo, Amarillo, Texas 79124.

The primary concern of the present decade is air pollution as aerosols in the form of particulate matter (PM), also known as particulate pollution. The most dangerous particulate matters are those measuring less than 10 μm since when inhaled, they can induce specific allergies and asthma. Improvement of indoor air quality is extremely important in order to maintain good health. This study focused on the identification and quantification of aeroallergens in the outdoor air of the Texas Panhandle and on the efficiency of AHPCO and Bi-Polar technologies (Air Oasis) on the decay of particulate matter. The aeroallergens were collected using a Burkard Volumetric Spore Trap (UK) placed on the third floor roof of the Agricultural and Natural Sciences Building at West Texas A&M University. The trap rotates with the direction of the wind and collects the aeroallergens on the Melinex tape placed on the drum. The tape was stained with 2% Safranin, examined, and photographed using a BX-40 Olympus microscope attached to a DP-70 Digital Camera. Image Pro Plus software was used to analyze the captured images and measurements (diameter and area) of the aeroallergens were recorded. This study focused on analyzing the two most common types of aeroallergens, fungal spores and pollen. The analysis was done for the 2015, 2016 and 2017 summer months. Lower amounts of pollen and mold were counted during months with higher precipitation. A constant high number of pollen and mold was observed in the summer of 2017 compared to the 2015 and 2016 summer months. Pollen of *Morus rubra*, *Platanus occidentalis*, *Geranium robertianum*, *Chenopodium sp.*, and *Pinus sylvestris*, and spores of *Alternaria sp.*, *Pithomyces sp.*, *Drechslera sp.*, *Cladosporium sp.*, and *Curvularia sp.* were identified. A fiberglass chamber was used to evaluate the rate of the decay of aerosol as a function of time before and after using the AHPCO nanotechnology in an air purifier 3000 and the plasma nanotechnology in a Bi-Polar unit. Illite NX powder was used as an aerosol sample since it has a similar mineralogical composition to atmospheric mineral dust. The 12 mg/m^2 of powder was dispersed in the chamber through an inlet. A DustTrack 8520 spectrometer was connected to the chamber to quantify the concentration and evaluate the rate of the decay of the dust particles over a time period. A higher rate of PM decay

was measured when using the Air Oasis units as compared to the control with no unit. AHPCO and Bi-Polar units degraded high and low concentrations of aerosol at similar rates of decay. Specifically for the experimental runs of high concentrations of particulate matter, the rate of decay was faster by $0.00049\text{mg}/\text{m}^3\text{s}$ with the Bi-Polar unit as compared to $0.0001\text{mg}/\text{m}^3\text{s}$ with the unit with AHPCO technology. This indicates the Bi-Polar unit was slightly more efficient in terms of reducing the concentration of the particulate matter in the indoor air. This technology can be used at various facilities like residential homes, hospitals, offices and restaurants to improve the indoor air quality by reducing the concentration of particulate matters present in the air.

SINGLE-MOLECULE IMAGING OF MOTOR PROTEIN MYOSIN IIIA USING TIRF MICROSCOPY. MUNENORI ISHIBASHI, TSUYOSHI SAKAI, REIKO IKEBE, and MITSUO IKEBE, Department of Cellular and Molecular Biology, UT Health Northeast, Tyler, Texas, USA

Over 60 years ago, when Watson and Crick discovered the DNA structure, people believed that advancing technology would bring us artificial intelligence under the form of robots that would be able to intellectualize and behave like humans. Huge technology advancements were achieved in the past 60 years, but humanoid robots like transformers are still beyond our grasp. That is probably because life systems (brains) use totally different principle than artificial machines. To understand the differences between biological machines and man-made ones, an important approach is to visualize and analyze single-molecule (protein) behavior at work in living cells. This study is an example of a single-molecule research, specifically of myosin IIIA, a motor protein. Stereocilia is an actin-based mechanosensing structure in the inner ear and plays an important role for auditory function. Myosin IIIA is localized at the tip of stereocilia and is important for their structural and functional integrity. Since myosin IIIA is an actin-based motor protein, it has been thought that it functions as a transporter of cargo molecules that create the structural and functional base of stereocilia. A critical but so far unanswered question is how myosin IIIA can transport its cargo molecules to contribute to the structure of stereocilia. The best approach to address this question is direct visualization of the movement of myosin IIIA. In this study, imaging of the movement at single-molecule level was achieved with TIRF microscope. HeLa cells were used as an *in vitro* reconstitution system (Fig. 1). Live-cell single-molecule imaging revealed continuous movement of Myosin IIIA towards filopodial tips at $\sim 120\text{ nm}/\text{s}$ of average velocity. The forced dimerization did not influence the velocity while the actin tethering at the C-terminal end of the tail was critical for the processive motor movement of myosin IIIA. Our results suggest that myosin IIIA walks along actin filaments as monomer by orchestration of both

motor and actin-binding domain. This work enhances our understanding of biophysical mechanism of myosin IIIA and provides important insights into its function in stereocilia.

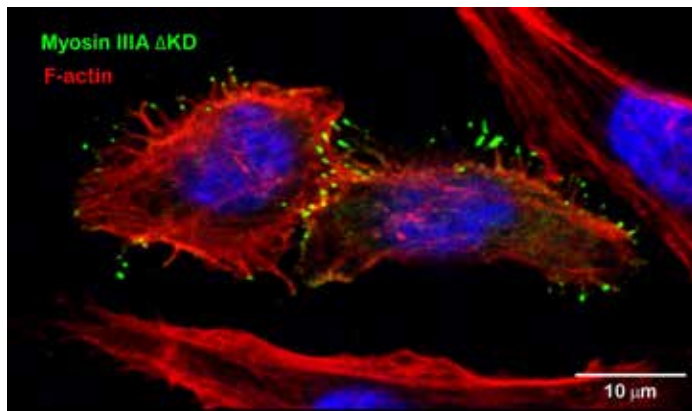


Fig. 1. Deletion of kinase domain (Δ KD) of Myosin IIIA (green) shows its localization at the tip of filopodia in HeLa cells.

CARIBBEAN CORAL: COMPOSITION AND SKELETON HIERARCHY. M. JOSEFINA ARELLANO-JIMENEZ, EDUARDO ORTEGA, ALEJANDRA LONDOÑO-CALDERÓN, and MIGUEL JOSÉ-YACAMÁN, Department of Physics and Astronomy, The University of Texas at San Antonio, San Antonio, TX 78249

Coral reefs contain a number of coral species that form unique systems. Caribbean scleractinian corals present two remarkable features: on one hand, they deposit a heavy exoskeleton of calcium carbonate in the crystallographic form of aragonite, and on the other hand, some hermatypic species extract calcium from seawater ten times faster in sunlight than in darkness. Previous studies about biomineralization support the hypothesis that the process starts with the formation of precursor nanoparticles that the animal deposits in an organic matrix. There is no conclusive evidence of this process in corals. The purpose of this work was to analyze the mineral phases present in coral, mainly the crystalline structure at nanometric scale. Energy Dispersive Spectroscopy (EDS) as well as X-Ray diffraction (XRD) and Selected Area Electron Diffraction (SAED) were used to identify elemental composition and mineral phases present in Staghorn coral (*Acropora cervicornis*, *Acroporidae*). Sections of the coral skeleton were made as shown in Fig. 1, embedded in PMMA, and polished for microstructural characterization. The structure of the coral surface shows two main regions as in spherular aggregates of crystallites and voids. EDS and XRD analysis show CaCO_3 as the main component, and the presence of Na, Mg, and Sr impurities. TEM analysis was performed on FIB lamellas from the plan view and cross section specimens (Fig. 1) and was used to identify the CaCO_3 phases. SAED patterns show that spherular structures are mainly composed of large aragonite crystals. Dark-field imaging was used to expose the presence of small vaterite

crystals inside the main aragonite structure in agreement with the XRD observations. These results can be relevant to verify the presence of calcium-carbonate nanoparticles as precursors of the biomineralization process in coral.

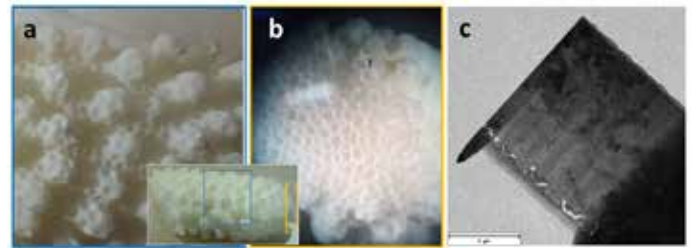


Fig. 1. Macro- and micro-scale images of a section of Staghorn coral (*Acropora cervicornis*). Optical microscope images from lateral (a) and top (b) regions show the characteristic morphology of the sample; the inset shows the full 5cm-long coral piece with the locations for imaging in (a) and (b). After sectioning, embedding, and polishing, FIB lamellas were prepared and subsequently analyzed with TEM. The low-magnification TEM image (c) reveals a wide distribution of crystal sizes in the selected regions of the sample.

METABOLISM AND AGGREGATION OF C-TERMINAL FRAGMENTS OF TAR DNA BINDING PROTEIN (TDP43). YASAR ARFAT T. KASU and CHRISTOPHER S. BROWER, Department of Biology, Texas Woman's University, Denton, Texas 76204-5799

Protein aggregation is a hallmark feature of neurodegeneration. It occurs either due to an increase in the production or a decrease in the removal of protein fragments. Previously, we have shown that Arginyl transferase 1 (ATE1) is involved in the degradation of aggregation prone and neurodegeneration associated proteins, $\text{A}\beta$, Tau, alpha-synuclein and C-terminal fragments of TAR DNA binding protein (TDP43) through the N-end rule pathway (Brower *et al.*, 2013). Current study dissects the differences in the metabolism and aggregation between two specific C-terminal fragments of TDP43, TDP43²¹⁹⁻⁴¹⁴ and TDP43²⁴⁷⁻⁴¹⁴, identified in the aggregates of amyotrophic lateral sclerosis (ALS) and dementia patients. We found that these C-terminal (almost similar) fragments differ in their ubiquitylation, dependency on N-end rule pathway for degradation, aggregation propensity, and aggregates morphology. Quantification of aggregates containing cells through the NIS elements software of a confocal microscope, showed higher levels of aggregation in CRISPR-mediated ATE1 knocked out cells for TDP43²⁴⁷⁻⁴¹⁴ than for TDP43²¹⁹⁻⁴¹⁴. We also have found that TDP43²¹⁹⁻⁴¹⁴ fragment made only 'dot-like' shaped aggregates, while the TDP43²⁴⁷⁻⁴¹⁴ aggregates were both filamentous and 'dot-like'. Furthermore, our data suggest involvement of an additional pathway in the degradation of TDP43C-terminal fragments. Future research will examine the toxicity exhibited by these fragments in wild type and CRISPR-mediated ATE1 knock-out yeast and mice cell lines. This research may be

helpful in understanding the causes of neurodegeneration, determining prognoses of ALS and dementia patients, and in designing therapeutics for neurodegenerative diseases.

CERAMIDES LOCALIZE TO THE CENTROSOMES AND GRANULES WITHIN THE P CELL OF *C. ELEGANS* EMBRYOS. SKYLAR D. KING and PAMELA A. PADILLA, University of North Texas, Department of Biological Sciences, 1155 Union Circle #305220, Denton, Texas 76203

Ceramides are composed of a sphingosine and a fatty acid. They have a structural role in the membrane of mitochondria and ER, as well as signaling functions. Disruption of the ceramide biosynthesis pathway has wide ranging impacts on biological processes including stress responses (e.g. O₂ deprivation, apoptotic signals in the germline, mitochondrial surveillance system), lifespan, and fecundity. In *C. elegans*, the *hyl-1*, *hyl-2*, and *lagr-1* genes code for ceramide biosynthetic enzymes. HYL-1 and LAGR-1 metabolize C ≥24 ceramides, whereas HYL-2 synthesizes C ≤22 ceramides. Simultaneous disruption of *hyl-1* and *hyl-2* results in lethality, clearly indicating that ceramide biosynthesis is an essential process for life. Our approach was to use indirect immunofluorescent staining, employing the anti-ceramide antibody, mAb 15B4, to examine the localization patterns of ceramides throughout *C. elegans* embryogenesis. Our initial findings using epi-fluorescent microscopy, proposed that the ceramide antibody localized to structures resembling the centrioles and granule-like perinuclear structures within the P cell throughout early embryonic development. *C. elegans* germline development begins in the embryo where asymmetrical segregation of the P cell lineage separates to germline blastomeres (P1-P4) during embryogenesis. Proteins specific to the germline, or P granules, sequester to the P cell maintaining maternally inherited macromolecules necessary for proper preservation of future generations. MEX-3 and PGL-1 have been established as such proteins. Using laser scanning confocal microscopy and MEX-3::GFP and PGL-1::GFP strains to visualize MEX-3 and PGL-1, it was determined that there is an overlap between the anti-GFP and mAb 15B4 localization pattern. Additionally, the mAb 15B4 also recognized centrosomes (marked by anti-γ tubulin). Surprisingly, the *hyl-2* mutant showed a loss of mAb 15B4 localization to the granule-like structures within the P cell but remained localized at the centrioles. Meanwhile, the *hyl-1;lagr-1* mutant displayed no loss of localization at either location, indicating that the mAb 15B4 antibody is recognizing an antigen in P granule composition that is dependent on the *hyl-2* ceramide biosynthesis pathway. These data suggest that ceramides localize to the centrosomes and P granules throughout *C. elegans* embryogenesis. These findings are significant because germline development allows the inheritance of traits, is a highly conserved process between metazoans, and is required to produce the next generation

of offspring. Given that ceramides are structural membrane components of mitochondria and ER and important signaling molecules, we are further investigating their function within the centrosomes and P cell during *C. elegans* embryogenesis.

IN VITRO DEVELOPMENT AND REPRODUCTION OF THE ENTOMOPARASITIC NEMATODE (EPNs) *STEINERNEMA CARPOCAPSAE* IN MONOXENIC LIQUID CULTURE. JEISON VALENCIA¹, DEVANG UPADHYAY¹, NABARUN GHOSH², SAMANTHA MCLEOD^{2*}, SIVANADANE MANDJINY¹, JEFF FREDERICK¹ and LEONARD HOLMES¹, ¹Biotechnology Research and Training Center, University of North Carolina, Pembroke, NC 28372, ²Department of Life Earth and Environmental Sciences, West Texas A&M University, Canyon Texas 79015

Steinernema carpocapsae (Fig. 1) is an entomopathogenic nematode used as a biological control agent for crop insect pests. A bio-control agent is a safe and healthy alternative to chemical pesticides. These nematodes can infect a wide range of insects that have a negative impact to farm lands while not causing harm to the beneficial insects or the soil. *S. carpocapsae* has a symbiotic relationship with *Xenorhabdus nematophila* bacteria. The nematode provides a route for the bacteria to get to pest insects, which will be killed within 24-48 hours. Thus, this symbiotic relationship is what makes *S. carpocapsae* a bio-control agent.

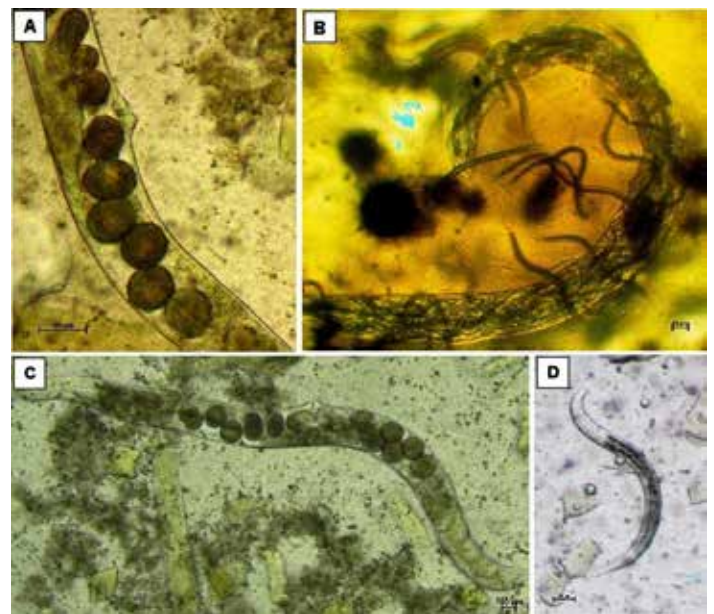


Fig. 1. Representative light microphotographs showing the developmental stages of *S. carpocapsae*; (A) Nematode maternal adult body with fully developed vulva and eggs, (B) Endotokia matricida stage nematode with infective juveniles (inside the body and released into the media), C: full sized nematode adult body, D: J2 stage nematode.

The current work involves studying the growth cycles and the mass production of the nematode using liquid culture fermentation technique. *Galleria mellonella* larvae were infested by the *S. carpocapsae* nematodes and the resulting

dead larvae were dissected to isolate *X. nematophila* from the hemolymph. There are several *in vitro* technologies used to mass produce this biological control agent. Mass production in liquid media is an ideal culturing method as it increases nematode yield and lowers production cost. Reproduction of *S. carpocapsae* was conducted by using a 5L Sartorius Stedim Biostat® fermentation system. In this batch culturing-process, 7.0×10^4 IJs/mL yield was achieved from 3×10^3 IJs/mL inoculum concentration after 13 days. In the bioreactor, it is possible to identify the different nematode life stages by the nematode's appearance and to calculate the percentage of each life stage.

NITROGEN CELL QUOTA VARIES SPATIALLY ALONG HETEROCYSTOUS CYANOBACTERIAL TRICHOMES EXPERIENCING N-LIMITED GROWTH.

FELICIA OSBURN* and THAD SCOTT, Department of Biology, Baylor University, Waco, TX 76706

When exposed to Nitrogen (N) limiting conditions, certain species of cyanobacteria are capable of transforming atmospheric N into usable ammonium (NH_4^+) using the enzyme nitrogenase. Under such conditions, some cyanobacteria differentiate specialized cells (heterocysts) from vegetative cells that maintain the intracellular hypoxia necessary for nitrogenase activity to occur. The advancement of Energy Dispersive X-ray Spectroscopy (EDS) with SEM has opened the opportunity to derive N cell quotas and stoichiometry (*i.e.* C:N ratios) on individual cells in cyanobacterial trichomes. To our knowledge, no research has quantified how fixed N is distributed spatially relative to heterocyst along the trichome. To see how fixed N is distributed along the filament, *Anabaena flos-aquae* (Fig. 1) was grown under N-limited conditions for multiple months to ensure N_2 fixation was occurring. Filaments were then air dried and examined using SEM which was equipped with EDS to analyze the elemental composition of individual cells. EDS gave values of N in atomic percent (%), which were used to compare differences in N quotas between the heterocyst and vegetative cells.

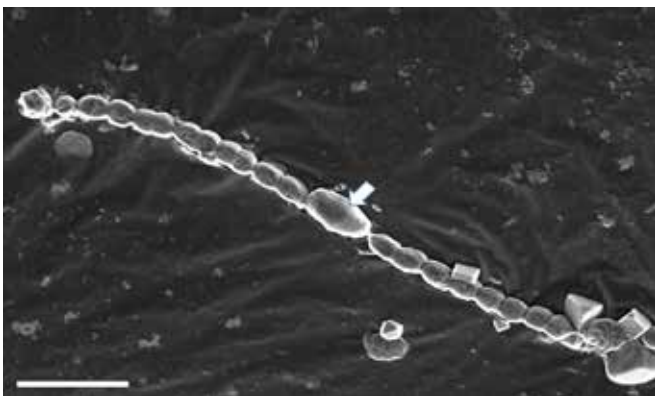


Fig. 1. Representative SEM-micrograph of a filament of *A. flos-aquae* with a heterocyst present (arrow). Samples were air-dried, sputter coated with carbon, and imaged with SEM at 5 kV (spot size 5) at a working distance of 13 mm. Bar=10 μm .

Lower N cell quotas occurred within the heterocyst (7.99% N), while approximately the same higher cell quotas of N were found in all vegetative cells from the terminal cell to the neighboring cell of the heterocyst (~11.69% N). This showed an increase of ~46% N between the heterocyst to vegetative cells. These findings suggest that while N is fixed within the heterocyst, the N quota of this cell is lower than that of the vegetative cells, possibly due to lower metabolic requirement as a lack of photosynthetic activity. As such, less N remains within the heterocyst once it is fixed and rather is distributed somewhat equally among the vegetative cells to support continued cellular functions. The results of this work will contribute to new studies on how *A. flos-aquae* distributes nutrients along the filament under N limiting conditions.

COOPERATIVE ACTIVATION OF STRIATED MUSCLE THICK FILAMENTS BY S2 BINDING. DUAA QUEDAN, ANDREA BERNARDINO-SCHAEFER, ROHIT SINGH, CHRISTOPHER THANG, MITHILESH BHASKARUNI, RITI SRIVASTAVA, and DOUGLAS D. ROOT, Department of Biological Sciences, Division of Biochemistry and Molecular Biology, University of North Texas, Denton, TX, 76203

Myosin binding protein C (MyBPC) is present at a very low ratio relative to myosin in muscle, yet it has a significant impact on contractility in cardiomyopathies. One explanation is that MyBPC cooperatively modulates the binding of the subfragment-1 (S1) to the subfragment-2 (S2) coiled coil. To test this hypothesis, the MF30 monoclonal antibody is used to compete with MyBPC for binding to S2. As a control, the MF20 monoclonal antibody which binds to light meromyosin does not affect muscle contraction. Expansion microscopy (Chen *et al.*, *Science* 347:543-8) of myofibrils reveals that MF30 but not MF20 has reduced labeling in the region of MyBPC binding consistent with competition between MF30 and MyBPC. Designed antiS2 synthetic peptides that modulate myosin S2 stability demonstrate cooperativity similar to MF30 with higher measured Kd values than their EC50 or IC50 on myofibril contractility. Furthermore, fluorescent labeling of the antiS2 peptides reduces their binding affinity but not the extent of their effect on myofibril contractility. The antiS2 peptide that destabilizes the coiled coil had a greater maximum enhancement of myofibril contractility than MF30, which suggests that the peptide may block the binding of S1 to S2, while MF30 may simply act by sterically blocking MyBPC. Furthermore, MF30 has no effect on *in vitro* motility assays of purified actin and myosin, while the destabilizing peptide slightly enhanced actin sliding velocities. These results support the view that a cooperative transition occurs between less active and more active conformations of myosin in the thick filament that can be modulated by a substoichiometric amount of effector. Implications for the design of drugs targeting muscle contraction will be presented.

LATICIFERS OF TEXAS NATIVE *EUPHORBIA* AND *CROTON* SPECIES. FATIMA RAZA* and CAMELIA MAIER, Texas Woman's University, Department of Biology, Denton Texas, 76204-5799

Species of *Euphorbia* and *Croton* (*Euphorbiaceae*) have been used by Native Americans for medicinal purposes. Exotic species of *Croton*, known for their red latex (Dragon's blood), are used as a "liquid bandage", by Amazonian native peoples. Most secondary compounds with medicinal properties in *Euphorbiaceae* species are found in laticifers, specialized cells producing latex, individualized cells (Fig. 1) or forming tubes and networks, in stems, leaves, and flowers (Castelblanque *et al.*, 2007). Despite the widespread of laticifers in the plant kingdom, studies on their structure and functions have lagged behind in recent years. This study aims to locate laticifers in six native *Euphorbiaceae* species: Snow-on-the-prairie, *E. bicolor*; Spotted Spurge, *E. maculata*; Prairie Tea, *C. monanthogynus*; Woolly Croton, *C. capitatus*; and Tooth-leaved Croton, *C. glandulosus*. Also, an exotic species, Garden Groton, *Codiaeum variegatum*, was studied for the presence and location of laticifers. The plant leaves were sectioned into small fragments and placed in FAA fixative overnight, after which they were washed with 70% ethanol and stained with Sudan Black B for 3-4 hours at room temperature. Afterwards, the fragments were washed with 70% ethanol and water, clarified in 2.5 M NaOH, and observed with an Olympus BH-2 light microscope equipped with a Nikon Digital Camera DXM1200. Laticifers in *E. bicolor* leaf and inflorescence bract were non-articulate, branched, but not interconnected (Fig. 1). *E. maculata* had a network of long, branched tubes which stained poorly with Sudan Black B. The latex in these non-articulate laticifers in both leaf primordia and mature leaves may have a different composition than *E. bicolor* latex.

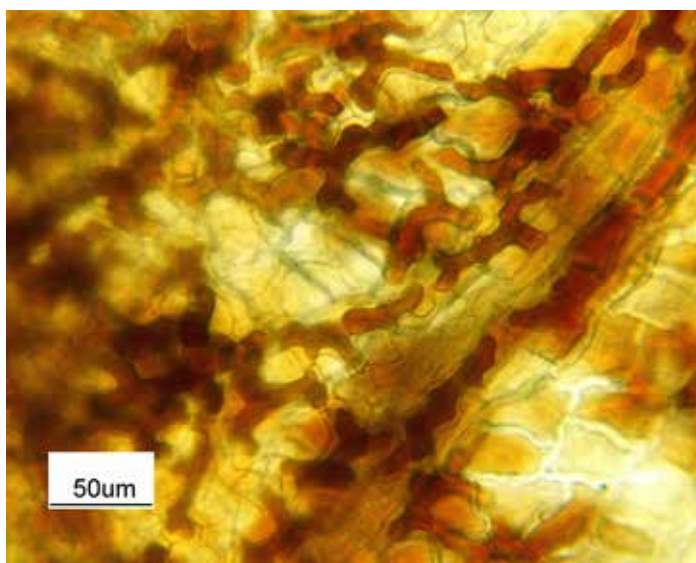


Fig. 1. Laticifers in *E. bicolor* bract stained with Sudan Black B.

Although laticifers were described in exotic *Croton* species, they were not present in *C. capitatus*, but the base of the

trichomes stained black with Sudan Black B. *C. glandulosus* and *C. monanthogynus* leaves showed individual stained cells containing druses surrounded by the black-stained material (idioblasts). The leaves of exotic ornamental Croton, *Codiaeum variegatum*, possessed a network of tubes throughout the leaves, faintly stained with Sudan Black B, as well as well-stained idioblasts with druses. To the best of our knowledge, this is the first study on the morphology and location of laticifers in *C. monanthogynus* and *C. capitatus*. Future work will focus studying laticifers in other plant organs, such as roots and stems.

RECEPTOR MEDIATED ENDOCYTOSIS OF SURFACE FUNCTIONALIZED NANOCARRIERS: EFFECT OF SIZE AND CHARGE IN NEURONAL UPTAKE. REMYA A. VEETIL¹, SUMOD SEBASTIAN¹, THOMAS MCALLISTER², SANTANEEL GHOSH² and DIANNA HYND¹, ¹Texas Woman's University, Denton, TX 76204, ²Southeast Missouri State University, Cape Girardeau, MO 63701

Traumatic damage to the spinal cord causes acute neuronal death and the inability of damaged neurons to regenerate their axons leads to persistent loss of function. Though there are several mechanisms known to encourage axon regeneration, the delivery of therapeutics and drug targeting to particular cell types in spinal cord is complicated by such factors as blood-spinal cord barrier. A nanodrug delivery system that specifically target dorsal root ganglion and/or corticospinal tract neurons and controls the release of therapeutic drugs is ideal for enhancing regeneration of damaged axons. Even though nanodrug carriers are promising, a thorough understanding of their neuronal uptake is critically important for further modifications. Cellular uptake of nanodrug carriers might occur through receptor mediated endocytosis (RME). In the present study, we analyzed the uptake of surface functionalized nanocarriers (SFNCs) in neurons through clathrin and caveolae-mediated endocytosis (CME and CvME). The effect of different SFNC sizes and charges were analyzed as well. We used -COOH and -NH₂ SFNCs of two different sizes (~150nm and 750nm) to study the mechanisms of cellular uptake in B35 neuroblastoma cells, PC12 pheochromocytoma cells and primary rat (P0) cortical neurons. Pharmacological inhibitors of clathrin, caveolae and dynamin were used to block RME of SFNCs. Different techniques like immunocytochemistry, confocal microscopy and live cell imaging were used in the study. Colocalization results showed that a proportion of the -NH₂, -COOH and -COOH750 SFNCs are internalized through CME or CvME. Reduction in SFNC-Early endosome correlation followed by inhibitor treatment revealed the role of endocytic mechanisms other than CME and CvME in SFNC endocytosis. Decrease in SFNC (TRITC) mean intensities of Pitstop1, Nystatin and OcTMAB treated cells indicated a significant reduction in the SFNCs internalized

through CME and CvME. Altogether, these results showed the feasibility of functionalized nanocarriers for targeted drug delivery to different neurons and their intracellular compartments to encourage axon regeneration following spinal cord injury. *Supported by TWU Department of Biology, The Southeast Missouri State University Department of Physics and Engineering Physics, and TWU Research Enhancement Program grants.*

THE ROLE OF AHPCO NANOTECHNOLOGY IN OCCUPATIONAL EXPOSURE CONTROL: REDUCING AIRBORNE DANDER CONCENTRATION IN THE ANIMAL LABORATORY. CHANDINI REVANNA¹, TODD ANDERSON¹, AUBREY HOWARD², JON BENNERT³, JEFF BENNERT³ and NABARUN GHOSH²
¹Department of Environmental Toxicology, Texas Tech University, Lubbock, Texas 79416, ²Department of Life, Earth and Environmental Sciences, West Texas A&M University, Canyon, Texas 79015, ³Air Oasis, Amarillo, Texas 79118

Mouse antigen has been associated with allergy asthma exacerbations. Mouse urinary and skin follicle proteins (lipocalin) are carried on small/large air borne particles/laboratory dust and dander. Studies have shown 11-44% occupational exposure related allergies among animal laboratory workers, of which 4-22% eventually developed occupational asthma. This study presents an evaluation of the efficiency of AHPCO nanotechnology in controlling airborne dander concentrations in the animal laboratory. We performed microscopic and aerosol sampling in an animal laboratory (mice laboratory in Human Sciences Building, Texas Tech University, Lubbock.), and analyzed the pre- and post-AHPCO air samples using the Air-O-Cell sampler. The Air-O-Cell sampler is designed to operate at an optimal flow rate of 15 liters per minute (lpm). An accredited laboratory (Sanair) was used for microscopic assessment of dander concentration in the laboratory before and after using the AHPCO technology. Sanair lab reported a gradual reduction in dander particle concentration sampled during specific intervals. The initial dander concentration was 2800 count/m³, which was reduced to 1013 count/m³ after 24 weeks of using the AHPCO nanotechnology, a statistically significant reduction (linear regression analysis; $p = 0.0006078$). For microscopy, samples were collected on double sticky tape placed on clean glass slides, stained with 2% Safranin, and observed with a BX-40 Olympus digital microscope. A graticule of 100 sq. micron area was calibrated with the 40x objective lens and dander particles inside that graticule area were counted. The Image Pro 6.0 software was used to record measurements of the dander particles. With the use of AHPCO, air and tape samples show significant reduction in dander count. The AHPCO nanotechnology can be used for air purification and to control occupational exposure to airborne dander in animal laboratory facilities.

NEURONAL DELIVERY OF Y27632 ROCK INHIBITOR USING NANOCARRIERS. SUMOD SEBASTIAN¹, REMYA A VEETIL¹, SANTANEEL GHOSH² and DIANNA HYND¹, ¹Texas Woman's University, Denton, TX 76204, ²Southeast Missouri State University, Cape Girardeau, MO 63701

Rho kinase (ROCK), known as Rho-associated coiled-coil forming protein serine/threonine kinase or Rho-associated kinase, is one of the central regulatory molecules for cytoskeleton control, cell adhesion process, and gene expression. ROCK II isoform of Rho kinase is preferentially expressed in brain. ROCKs are downstream effectors of RhoA GTPase in axonal growth inhibition causing rapid growth cone collapse, neurite retraction, and neurite growth inhibition. ROCK up-regulation has been found in spinal cord injury. It has been reported that ROCK inhibitors were able to improve neural function recovery after nerve damage or after brain ischaemia/reperfusion injury in animals. One ROCK inhibitor that has been widely used in axon growth and regeneration research is Y-27632, which specifically inactivates ROCK. Y-27632 promotes growth of neurites, both on permissive substrates and on growth inhibitory substrates. In the present study, we treated B35 neuroblastoma cells with different concentrations of Y-27632 and quantified the neurite outgrowth using a Nikon A1 confocal microscope system. Also, we have developed a biocompatible polymer encapsulated magnetic nanocarrier system (PE-MNC) for neuronal drug delivery. In the current study, treatment with 1 μM to 400 μM of Y-27632 showed significant increase in the length of longest neurite per axon. Moreover, total neurite length showed significant increase with 0.8 μM to 400 μM Y-27632 treatment. Based on these results, in future studies we will be loading PE-MNCs with Y-27632 to get a releasing concentration of 50 to 400 μM in rat cortical neurons. *Supported by TWU Department of Biology, The Southeast Missouri State University Department of Physics and Engineering Physics, and TWU Research Enhancement Program grants.*

TESTOSTERONE MAY ACT DIRECTLY ON GERM CELLS VIA NON-CANONICAL MEMBRANE PROGESTERONE RECEPTORS AS WELL AS ON SOMATIC CELLS ARPITA TALAPATRA^{*1}, DIBYENDU DUTTA² and NATHANIEL MILLS¹, ¹Texas Woman's University, ²Middle Tennessee State University, Murfreesboro, Tennessee

Testosterone, having high concentration in testes, can act either through canonical - nuclear receptors or may act through non-canonical membrane receptors that influence cytoplasmic cellular functions instead of gene regulation. Progesterone, a steroid hormone regulating female reproduction by nuclear receptors, can change ion influx and intracellular Ca²⁺ via second messenger - non-genomic pathways mediated by membrane progesterone receptors (mPRs) also known as progestin-adiponectin receptors (PAQRs) similar to receptors (AdipoR1 and

AdipoR2) for adiponectin from fat. At least five mPRs (PAQRs) are known and have no structural/amino acid sequence homology to nuclear steroid receptors. mPRs exhibit seven transmembrane domain comparable with G-protein coupled receptors (GPCRs) and the non-canonical pathway is thought to control G-protein cAMP cascades in reproductive tissues. Immunostaining indicated that androgen receptors (AR) are found in Sertoli cell nuclei, and myoid cell nuclei of the seminiferous tubule. Some staining in the stripped cytoplasm of spermatids, despite the fact that germ cells are reported not to have androgen receptors. We have initiated RT-qPCR studies in mature Sprague Dawley rats to find and characterize testicular mRNAs for membrane progesterone/ adiponectin receptors (mPAQRs). At least 5 mPR mRNAs [Paqr(s)] were found expressing in rat testes but the cellular origin of the RNA is unknown since using total RNA from whole testes was used. Our results suggest that the levels of mPRs are dependent on the level of testosterone. Currently, germ cell suspensions are stained with fluorescent labeled testosterone and progesterone to potentially identify an alternate pathway (mPRs) of testosterone action that may reveal germ cells to be direct targets of testosterone. *Supported by a Texas Woman's University Research Enhancement Program grant.*

LEVEL OF TESTOSTERONE NOT ONLY DETERMINE GERM CELL MORTALITY RATE VIA THE CANONICAL PATHWAY BUT MAY TRIGGER NON-CANONICAL PATHWAYS INVOLVING MEMBRANE PROGESTERONE RECEPTORS. ARPITA TALAPATRA^{*1}, DIBYENDU DUTTA², SAMUEL SANG³, NATHANIEL MILLS¹, ¹Department of Biology, Texas Woman's University, Denton, Texas, ²Middle Tennessee State University, Murfreesboro, Tennessee, and ³AIT Laboratories, Denton, Texas

Apoptosis, characterized by shrinkage of total cell volume, increased cell densities and compaction of cell organelles, is an important regulatory process during spermatogenesis. Male Sprague Dawley rats were injected with ethylene dimethane sulfonate (EDS) (75 mg/kg body weight) to selectively eliminate mature Leydig cells, thus ablating the source of testosterone. The TUNEL assay and analysis of gene expression modulated by testosterone was assessed 7 days post-EDS. To substantiate the role of testosterone, separate rat groups received exogenous testosterone for either supplementation or replacement of testosterone post-EDS. Significant germ cell apoptosis in EDS-treated rats was observed by the TUNEL assay and testosterone replacement prevented the germ cell apoptosis. The levels of pro- and anti-apoptotic genes of the *Bcl2* family in testes were determined by RT and qPCR after 7 and 10 days treatment. Members of the *Bcl2* superfamily are actively involved in the apoptotic pathway controlling cytochrome c release from mitochondria. These proteins share conserved α -helical BCL-2 homology (BH) domains 1-4. The BH3-domain has been marked as the minimal

death domains required to bind with other multi-domain *Bcl2* members. A significant increase in pro-apoptotic *BAK-1*, *BAD*, *BAX*, *BIK*, *BMF* and *BOK* and anti-apoptotic *BclW*, *Bcl2*, *BclXL* and *Mcl1* genes in testes of EDS-treated rats was found. All members possessing the BH3-domain were found to be regulated by testosterone, whereas *Bcl2L10* (no BH3 domain) remained unchanged. *Bcl2L10* is known to form heterodimers with *Bcl2* rendering anti-apoptotic activity. Fas and FasL increased while caspases exhibited variable levels. We observed germ cell detachment from Sertoli cells that exhibited cytoskeletal disorganization. Bioinformatics and computational tools were used to target the sequence of specific domain of *Bcl2L10* involved in interactions with *Bcl2*. Sequence alignment studies compared different interacting domains in the *Bcl2* superfamily to help in understanding the molecular mechanism of germ cell apoptosis. Immunostaining indicated that androgen receptors (AR) are found in Sertoli cell nuclei, and myoid cell nuclei of the seminiferous tubule along with some staining in the stripped cytoplasm of spermatids, however, germ cells are reported not to have androgen receptors. Testosterone receptor (AR, NR3C4) and progesterone receptor (PR, NR3C3) are structurally similar and testosterone at double the progesterone concentration will compete with progesterone for progesterone receptor activation. Fluorescently labeled testosterone and progesterone are being used to identify an alternate pathway (mPRs) of testosterone action that may show germ cells to be a direct target of testosterone. To characterize mPR mRNAs-membrane progesterone/adiponectin receptors (mPAQRs) by RT-qrtPCR, initial work revealed 5 mPR mRNAs [Paqr(s)] expressed in testes, however, the germ cell(s) of origin cannot be specifically identified by this method using total RNA from whole testes. To identify specific germ cells that bind testosterone at membrane receptors, cell suspensions will be prepared from mature EDS treated animals to remove *de novo* testosterone. Fluorescently labeled testosterone or progesterone will be used to probe for membrane binding while DNA/nuclear labeling will be identified by microscopy. Alternately, antibodies to the mPRs may be used to identify cells with these receptors from paraffin embedded samples. *Supported by a Texas Woman's University Research Enhancement Program grant.*

MATERIALS SCIENCE Spring 2018

EFFECT OF DRAWABLE CNT FOREST STRUCTURE ON RESULTANT CNT WEB PROPERTIES. ARIANA NAWABY, CHI HUYNH, and RAQUEL OVALLE, Lintec of America, Inc.- Nano Science and Technology Center (NSTC), Richardson, Texas

Highly aligned carbon nanotube (CNT) forests can be

grown using a chemical vapor deposition (CVD) process. When pulled, these forests yield an array of drawable, conductive CNT sheet or cSilk®. Due to the superior physical and electrical properties of these sheets, they have potential use for many applications. The characteristics of the CNT forests expectedly play a large role in determining those physio-electric properties. By investigating the effect of forest morphology on the resultant sheet, the ideal CVD product can be envisioned, thus facilitating optimization of the process. Properties of CNT forests are determined by height and density. CNT sheets are evaluated based on sheet resistance, transparency, and inter-bundle spacing. SEM was used to visualize a cross section of the CNT forest and thereby determine its height. (Figs. 1 and 2)

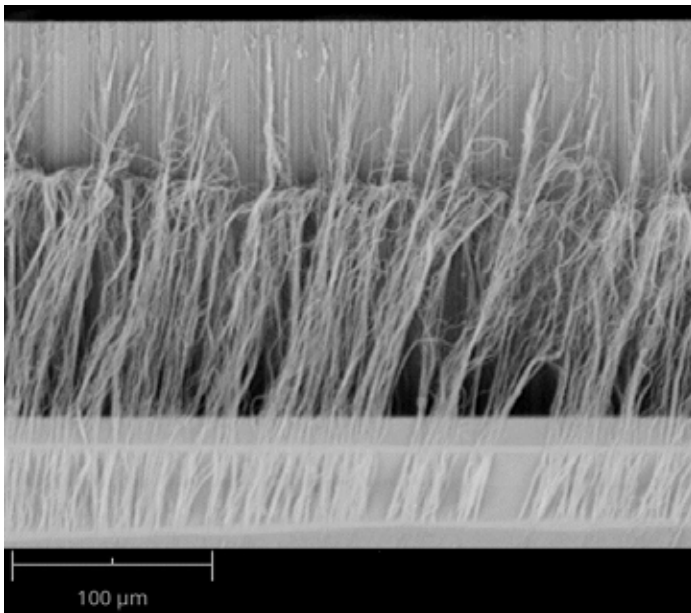


Fig. 1. Cross section of CNT forest with web fibers extending outwards.

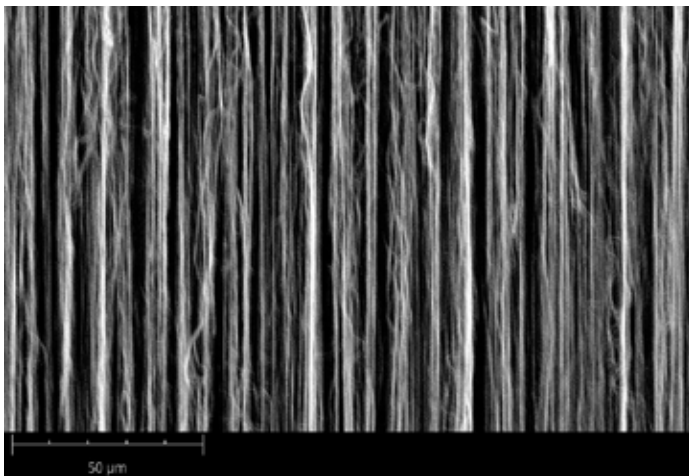


Fig. 2. Section of CNT web fibers.

Results showed that taller, denser CNT forests produced lower resistance nanotube sheets. The morphology of the nanotube sheet was subsequently analyzed using SEM

to better understand this trend. The gap spacing between bundles in the sheet was quantified as a percentage of the total sheet area. Fewer gaps were seen to correspond with a lower sheet resistance. Taller forests produced fewer inter-bundle gaps than shorter forests. The bundles in taller forests were also thicker than those seen in their shorter counterparts. This suggests that the conditions allowing for taller nanotube growth contribute to increased agglomeration of nanotubes during sheet drawing, thereby enhancing their conductivity.

POLYTYPOISM AND OPTICAL ANISOTROPY IN 2D TELLURIUM. ELISABETH BIANCO*¹, AMEY APTE², P.M. AJAYAN^{1,2}, and EMILIE RINGE^{1,2}, ¹Department of Chemistry, Rice University, Houston, TX 77005 USA, ²Department of Materials Science and NanoEngineering, Rice University, Houston, TX 77005 USA

Two-dimensional (2D) materials, which are only one or a few atoms thick, can possess exciting and tunable optical/electronic properties unique from their 3D counterparts, providing a platform to tailor physics through chemistry and engineering. Structure-property relationships in 2D materials, including the room-temperature quantum Hall effect in graphene, have inspired the search for new 2D materials. Amongst the newest class of ultrathin materials are those from non-layered parent crystal structures, like borophene. Here, we show the existence of 2D and quasi-2D allotropes of tellurium, another non-layered parent structure. We demonstrate two growth routes, physical vapor deposition and vapor transport, to achieve ultra-thin (<6 nm) Te films and tri-layer tellurene. These are robust toward oxidation and exhibit the $P3_121$ structure of p-type semiconducting Te - the only evidence of a hexagonal 2D Te allotrope to date. Transmission electron microscopy (TEM) and energy dispersive X-ray spectroscopy (EDS) confirm the composition and orientation of the films.

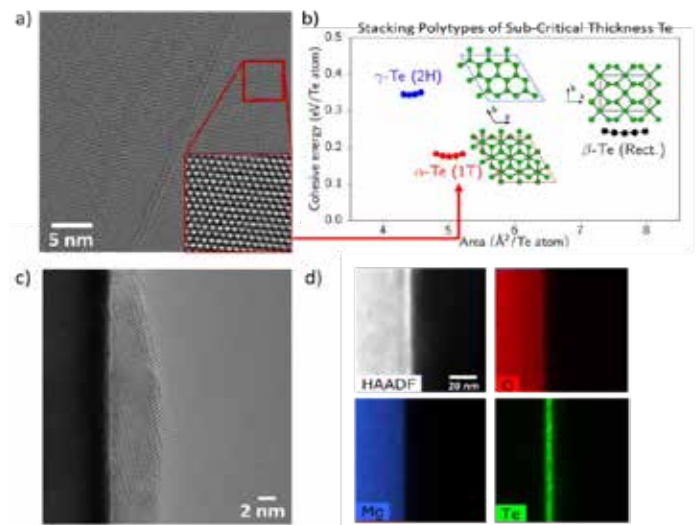


Fig. 1. Structure and composition of ultra-thin Te. a) TEM micrograph of tri-layer α -tellurene; b) Schematics of possible low-dimensional Te stacking polytypes; c) TEM micrograph and d) corresponding EDS data of ultra-thin Te films.

Furthermore, TEM and scanning transmission electron microscopy (STEM) reveal unique polytypism in the case of tri-layer tellurene. Polarized Raman spectroscopy and TEM unravel a correlation between optical anisotropy in ultra-thin Te films and tunable texturing/orientation. The orientation of the films can be manipulated by changing substrate, providing a rational handle for controlling optical properties in this new ultra-thin material. Optical tunability in ultra-thin Te and the discovery of a novel polytype of tellurene are significant toward the realization of 2D optoelectronics.

EVALUATION OF ABSORPTION CAPACITY OF NANOCOMPOSITES ON THE BASIS OF NATURAL PRODUCTS FOR OIL SPILL CLEANUP. JAVIER S. ACEVEDO CORTEZ, LIZBETH MARROQUÍN TIJERINA, THELMA SERRANO QUEZADA, YOLANDA PEÑA MÉNDEZ, OXANA V. KHARISOVA, BRENDA GÓMEZ LOMELÍ, VICTOR M. JIMÉNEZ PÉREZ, and BORIS I. KHARISOV*, Universidad Autónoma de Nuevo León, Av. Universidad, Ciudad Universitaria, C.P. 66455, San Nicolás de los Garza, Nuevo León, México. E-mail bkhariss@hotmail.com.

Natural sorbent materials have practical advantages for oil spill cleanup, such as their low-cost, feasibility for real-life applications and environmental adaptability. In this work, the absorption capacity was determined for natural plants such as *aloe*, *nopal* (Mexican cactus) and for *agar* after proper lyophilization (freeze-drying), as well as for their composites with silica, Fe₃O₄/polyesterene and multi-wall carbon nanotubes (MWCNTs). The worm-based (*Bombix Mori*) silk (flexible, resistant and hydrophobic natural polymer) and magnetic γ -Fe₂O₃/MWCNTs composites were also used. Freeze-drying of *aloe*, *nopal* and *agar* was performed in order to preserve the structure and increase the internal volume of sorbents. The structures of lyophilized sorbents and composites were analyzed with SEM, which showed the 3D arrangement with high-surface-area cavities in these biological materials that allowed for oil absorption. The composites with silica, Fe₃O₄/polyesterene and MWCNTs kept the 3D structure and exhibited coupling between both counterparts, natural material – SiO₂, Fe₃O₄/polyesterene or MWCNTs. The absorption capacities of *aloe*, *nopal* and *agar* were found to be 9 g/g, 3 g/g, and 26 g/g, respectively without any pre-treatment. Composites with Fe₃O₄/polyesterene had absorption capacities of 5.8 g/g, 2.8 g/g, and 14 g/g, respectively, and MWCNT composites had capacities of 7.8 g/g, 2.9 g/g and 23 g/g, respectively. Significant differences in adsorption capacity between lyophilized sorbents and composites have been attributed to lyophilization treatment allowing a better absorption of oil, water and other compounds. Absorption was found to be a more selective process for composites, since the hydrophobization excludes water absorption. For silk-based and γ -Fe₂O₃/MWCNTs composites, the oil remediation

efficiencies were observed in the 95-99% range. Despite the decreasing of absorption capacity of hydrophobic substrates, they are interesting materials for oil-spill cleanup application since they exhibit affinity for oil sorption. Being indeed low-cost wastes (especially *nopal*), these materials could be extensively used at the sites of oil spills of distinct scales, from small to catastrophic. The composites developed in this work have a considerably lower cost (less than 0.03 USD per 1 L of absorbed crude oil from its mixtures with water at different ratios) compared to classic absorbents, generally used for water-oil separation, such as aerogels and xerogels (approximately 200-300 USD per 1 L of absorbed crude oil).

MICROSTRUCTURAL ANALYSIS OF ER:YAG POLY-CRYSTALLINE CERAMIC USING CRYSTAL ORIENTATION MAPPING. DAVID SANCHEZ, EDUARDO ORTEGA, DHIRAJ SARDAR and ARTURO PONCE, Department of Physics and Astronomy, University of Texas at San Antonio, San Antonio, Texas 78249

The goal of this study was to characterize the morphology and composition of the grain boundaries (GBs) in a polycrystalline ceramic microstructure of Erbium (Er) quoted as 50 at. % in Yttrium Aluminum Garnet (YAG). The sample was prepared using a focused ion beam (FIB) dual beam microscope Zeiss model 340 cross beam and analyzed with a JEOL 2010F TEM operated at 200 kV and a JEOL ARM200F aberration-corrected scanning transmission electron microscopy (Cs-STEM) operated at 200 kV. X-ray energy dispersive spectroscopy (EDS) was performed for chemical quantification of the sample and the grain boundaries.

This work proposes that the high quantum efficiency seen in polycrystalline ceramics is due to the chemical segregation of Er at the grain boundaries. Figure 1a shows the sample prepared by FIB, in which four grains are observed. The analysis was performed in the grains labeled as I and II. Figure 1b shows a Z-contrast image registered using the high angle annular dark field detector (HAADF) in STEM mode. HAADF-STEM image confirms a higher concentration of Er (higher atomic number) at the GB compared with grains I and II in which Er:YAG alloy is present in the same contrast. Energy dispersive X-ray spectrometry (EDS) was carried out at the GB and in grain II to quantify Er concentration (Fig. 1e). A higher concentration of Er than Y was measured at the GB (Table 1). Selected area electron diffraction patterns (SAED) have been obtained in the individual grains. As an example, SAED patterns of grains I and II are shown in Figure 1c and 1d, respectively. The two patterns are oriented along two zone axes $\langle 213 \rangle$ and $\langle 113 \rangle$, which are 14.75 degrees misoriented from each other. To characterize the predominant angles in the GBs, a full crystal orientation mapping in the polycrystalline sample using automatic crystal orientation maps (ASTAR) assisted by the precession electron diffraction technique coupled to

the transmission electron microscope was obtained. Off-axis electron holography shows how the retrieved phase changes at the interfaces.

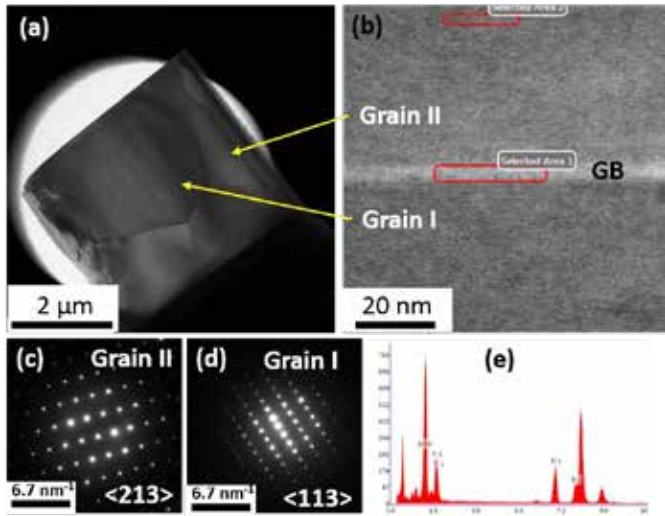


Fig. 1. Microstructure, chemical and structural characterization of Er:YAG. (a) TEM micrograph of the polycrystalline Er:YAG sample, (b) HAADF-STEM image indicating the selected regions for the EDS analysis, (c) and (d) SAED patterns of grains I and II indicated in Figure 1b, (e) Representative EDS spectrum.

Element	Atomic %	
	Area 1	Area 2
Er _{Lα}	58.12	57.74
Y _{Kα}	41.88	42.26

Table 1. Quantitative analysis of the EDS spectra collected in selected areas 1 and 2 marked in Fig. 1b.

ELUCIDATING MORPHOLOGICAL CHARACTERISTICS OF CELLULOSE MATERIALS. MARINA R. MULENOS* and CHRISTIE M. SAYES, Department of Environmental Science, Baylor University, Waco, TX, USA

Production and use of cellulose materials are continuing to increase in many industries, such as paper, cosmetics, and food. With the increase in production volumes, it is necessary to characterize the quality of products to ensure proper safety assessments. In terms of human health, both exposure and hazard data of chemicals and materials are of key importance to consumers and occupational workers. Before exposure and hazard data is collected, the physicochemical characteristics of materials should be reported.

To characterize cellulose materials, morphological information is imperative and microscopy is the best tool to collect data. In this study, three different cellulose materials, each collected from different industrial processes, were studied with light and electron microscopy techniques. The key physical characteristics analyzed were fiber length and width, aggregation, crystallinity and chemical impurities.

The cellulose materials were found to be fibers with a width range of 2-200 nm and length range of 0.5-10 μm. Each material had a different aggregation potential, extending beyond the individual fiber lengths. Sample C showed the most aggregation and sample B showed the least aggregation (Fig. 1). Transmission electron micrographs depicted samples B and C as fibers with little to no impurities. Dark-field microscopy highlighted a high mineral content in sample A, which was confirmed by X-ray dispersive spectroscopy and electron diffraction.

For the cellulose materials, it is hypothesized that changes in aggregation state can have an effect on the width and length metrics, which are important attributes when assessing bioavailability. Even though all three materials are cellulose-based, it was seen that each material possesses a different size profile, elemental composition, and possible exposure potential. The results of this study suggest that each manufactured cellulose material type must be characterized for physical and chemical features before commercialization.

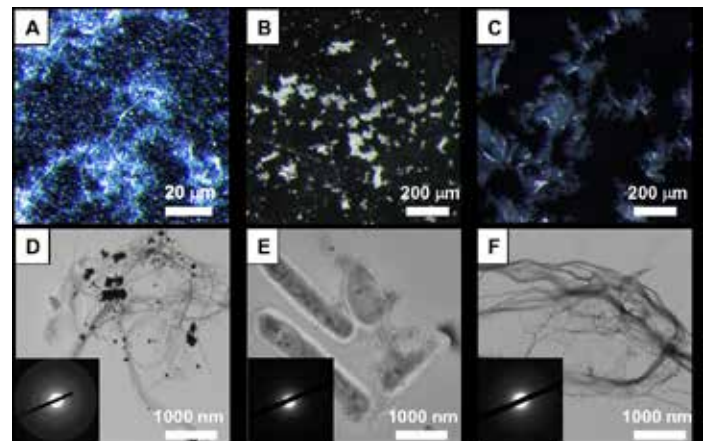


Fig. 1. (A-C) DFM images of three different cellulose materials. Panel A contains highly reflective materials possibly indicating crystallinity. (D-F) TEM micrographs of the corresponding cellulose materials in A-C. Mineral deposits, easily seen in panel D, show a distinct electron diffraction pattern, and could explain the high reflectivity in the corresponding DFM. All samples contain a mixture of fiber sizes (<1 μm to >20 μm).

EMPLOYING ELECTRON HOLOGRAPHY FOR THE STUDY OF MAGNETIC ORDERING IN TEMPLATES OF METALLIC NANOWIRES. EDUARDO ORTEGA*, ERIK PEREZ AND ARTURO PONCE, Department of Physics and Astronomy, University of Texas at San Antonio, San Antonio, Texas 78249.

Magnetic nanostructures have potential to improve current technologies, such as data storage and electromagnetic sensing. The magnetization behavior of thin ferromagnetic nanowires is dominated by the competition between magnetocrystalline anisotropy and shape anisotropy. This way, electron diffraction methods can be used to relate the crystallinity of thin ferromagnetic

nanowires with their observed magnetic behavior. High resolution crystal orientation mapping can be attained by using scanning-assisted precession electron diffraction (PED), which is based on the diffraction patterns collected from a precessed (conical) beam. The analysis of the magnetic behavior and its quantitative measurements can also be obtained inside the TEM using off-axis electron holography (EH). The retrieved phase from holography contains information about: thickness, electric potential, lattice distortion and magnetic fields. The combination of both techniques provides information of the magnetization as function of the grains/domains orientations in a polycrystalline structure. Moreover, using EH under Lorentz conditions we can experimentally determine the magnetization distribution over individual nanowires, and their interaction with neighboring nanostructures within the material-template composite. As an example, a previous work by the authors showed the dominant antiferromagnetic arrangement among a single row of nickel nanowires (Ni-NWs) within the alumina template (Ortega *et al.*, 2018). The magnetic induction image in Fig. 1 is obtained from the phase gradient and weighted amplitude retrieved using the inset electron hologram. The phase shift between opposite parallel directions (green/magenta) corresponds to a magnetization of 5.5×10^5 A/m. Using EH, we can visualize the ferromagnetic ordering within the nickel columns, where both simulations and experimental images show a curling mode due to the adjacent nickel layers.

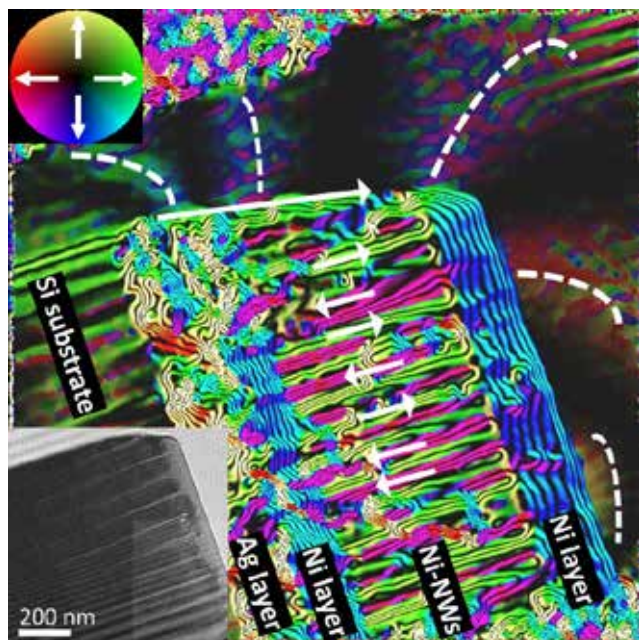


Fig. 1 - Amplification of the magnetic/electrostatic contour lines representing phase variations through the plane of the sample after an external H (~ 18 kOe) was applied perpendicular to the Ni-NWs.

FABRICATION OF CARBON NANOPARTICLES VIA THE SPRAY PYROLYSIS METHOD USING METAL PHTHALOCYANINES AS CATALYST PRECURSORS. OXANA KHARISSOVA¹, ANTONIO ALANIS¹, SERVANDO AGUIRRE TOSTADO², BEATRIZ ORTEGA GARCÍA³, HUGO GALINDO¹, and IDALIA GÓMEZ DE LA FUENTE³, ¹FCFM, Universidad Autónoma de Nuevo León, Av. Universidad S/N, Ciudad Universitaria, San Nicolás de los Garza, N.L., C.P. 66455, ²CIMAV, Parque de Investigación e Innovación Tecnológica. Apodaca, N. L., C.P. 66600, and ³FCQ, Universidad Autónoma de Nuevo León, Av. Universidad S/N, Ciudad Universitaria, San Nicolás de los Garza, N.L., C.P. 66455, México

In this work, the synthesis of carbon nanoparticles was carried out *via* spray pyrolysis using toluene-ethanol solution with suspended zinc, copper, nickel or magnesium phthalocyanines (MPc) as precursors of metallic particles serving as catalysts for carbon phase formation. Using MPc (M = Cu, Ni, Mg, Zn) as precursors, carbon thin films were prepared by a spray-pyrolysis technique using the powders of MPc dispersed in a mixture of toluene and EtOH or, alternatively, in a solution of ferrocene in toluene. The chosen MPc concentrations were 0.05 wt.%, 0.5 wt.% and 1 wt.%. Solvent [20 mL, toluene and alcohol (1:1)] and MPc or solution [20 mL, toluene and ferrocene (0.05 wt.%)] and MPc were injected into the system at a rate of 1 mL/min in a preheater set to 2000°C while nitrogen gas was supplied at a ratio of 1 L/min. After the preheating stage, the gas passed into a quartz tube which entered in an oven heated at 760-800°C. The quartz tube contained borosilicate glass substrates, on which thin nanofilms were deposited in 20 min. As a result, corresponding metal-containing multi-(MWCNTs) and single-(SWCNTs) wall carbon nanotubes formed. The samples were analyzed by SEM, TEM, FTIR-spectroscopy, UV-vis spectroscopy and their conductivity was measured *via* the Kelvin technique. The properties of formed nanolayers were analyzed according to metal nature in the phthalocyanine, temperature, carrier gas speed, and other process parameters. The diameter of SWCNTs, was found to be 1.45 nm. Thin layers of nanomaterials, deposited on borosilicate glass, were found to conduct at nanoampere scale. The deposited material was present on both sides of the substrate or on one side only. Among other results, the nanotubes obtained with magnesium and nickel phthalocyanines used as precursors were homogeneously distributed and have diameters of 20 nm and 750 nm for, respectively. This study shows that classical metal phthalocyanines can serve as catalyst precursors and carbon source at the same time in the formation of carbon nanotubes.

STUDY OF THE HYDROPHOBIC AND MECHANICAL PROPERTIES OF CELLULOSE, PREPARED FROM SOYBEAN HULLS, AND PAPER FIBER BASED ON KRAFT-TYPE CELLULOSE. BLANCA I. MONTES MEJIA¹, OXANA V. KHARISSOVA¹, and BEATRIZ ORTEGA GARCÍA², ¹FCFM, Universidad Autónoma de Nuevo León, Av. Universidad S/N, Ciudad Universitaria, San Nicolás de los Garza, N.L., C.P. 66455, México and ²FCQ, Universidad Autónoma de Nuevo León, Av. Universidad S/N, Ciudad Universitaria, San Nicolás de los Garza, N.L., C.P. 66455, México

It is known that natural polymers present in plants are promising materials for the development of hybrid coating systems. Natural polymer matrixes reinforced with different nanoparticles, for example SiO₂ or TiO₂, are of interest for possible applications as non-expensive hydrophobic materials. In particular, husk soy, as a byproduct of soybean oil production, containing approximately 40% fiber, has potential applications in the paper industry. The goals of this study were to obtain high-value micro- and nanocellulose from industrial wastes and to reinforce as well as to hydrophobize them with nanoparticles for the enforcement and improvement of the Kraft paper properties. Alkaline treatment with NaOH solution (10 wt.%) and acidic treatment using HNO₃ (65 wt.%), with further washing, filtering and drying, led to the formation of soy husk micro- and nanocellulose with particles of distinct sizes. The obtained samples were analyzed by infrared spectroscopy (IR), scanning electron microscopy (SEM), and transmission electron microscopy (TEM) and contact angles determined. Cellulose reinforced with SiO₂ nanoparticles (20 nm in size) in Kraft paper led to an increase of up to 86% in the mechanical properties of the paper, avoiding absorption of moisture, and forming water contact angles of 120° to 150°C. The functionalization of husk soy cellulosic fibers with nanoparticles generated a superhydrophobic material with apparently unique surface characteristics. This method has the potential to be used to replace the cellulose obtained from trees with low-cost soy bean industrial wastes, thus contributing to environmental conservation.

STRUCTURES OF NANOTUBES DECORATED WITH NANOPARTICLES OF STRONTIUM ALUMINATE DOPED WITH RARE-EARTH ELEMENTS. PATSY Y. ARQUIETA GUILLÉN¹, ALENA BORISOVNA K.², BEATRIZ ORTEGA GARCÍA³ and OXANA V. KHARISSOVA¹, ¹FCFM, Universidad Autónoma de Nuevo León, Av. Universidad S/N, Ciudad Universitaria, San Nicolás de los Garza, N.L., C.P. 66455, México, ²FIME, Universidad Autónoma de Nuevo León, Av. Universidad S/N, Ciudad Universitaria, San Nicolás de los Garza, N.L., C.P. 66455, México, ³FCQ, Universidad Autónoma de Nuevo León, Av. Universidad S/N, Ciudad Universitaria, San Nicolás de los Garza, N.L., C.P. 66455, México

In recent years, multi-wall carbon nanotubes (MWCNTs) have been studied for the purpose of finding new biosensors with fluorescent properties. The main goal of this study was to prepare fluorescent composites of carbon nanotubes and Ln-doped inorganic salts. In this work, the preparation of carbon nanotubes with fluorescent properties by means of spray pyrolysis is presented. The synthesis, structural properties, and applications of nanotubes, nanobuds and related nanostructures are detailed. An excellent ceramic material, SrAl₁₂O₁₉ was chosen to be combined with carbon nanotubes in order to verify the fluorescent property of the final composite. Some rare-earth elements ions were added to change the emission spectra of SrAl₁₂O₁₉ under UV irradiation. The synthesis was carried out on the surface of optical fibers to obtain a uniform growth of “forest”-type MWCNTs, by adding metal (M) oxide nanoparticles (M = Sm, Eu, Nd, La, and Ce) to SrAl₁₂O₁₉ surface. The MWCNTs decorated with strontium aluminate and doped with rare-earth elements were synthesized from different organic precursors and the corresponding metal oxides. The composites were characterized by XRD, SEM, TEM, FTIR spectroscopy, Raman spectroscopy and UV/visible spectroscopy. The analysis of the obtained data showed that the deposited nanoparticles are in the 20-60 nm size range, uniformly distributed on the MWCNTs surface. The samples prepared at different temperatures and doped with metal oxides on SrAl₁₂O₁₉ showed different fluorescence behavior. In particular, the metal ions with the best deposition (uniform coating) on the SrAl₁₂O₁₉ surface were found to be lanthanum and cerium. It was also assumed that the highest conductive materials are those doped with Nd, Eu and Ce, while the carbon nanotubes with La and Sm showed a higher presence of the SrAl₁₂O₁₉ on the CNT surfaces. All five used metals showed fluorescence under UV light. We achieved changes in fluorescence intensity in the final CNTs- SrAl₁₂O₁₉-M composites depending on the nature of added ion.

WATER-SOLUBLE PHTHALOCYANINE DERIVATIVE AS A NON-STANDARD GRAPHITE “DESTROYER” FOR GRAPHENE PREPARATION. OXANA KHARISSOVA¹, JARED RODRÍGUEZ¹, BORIS KHARISOV², and SANTOS A. CASTILLO SÁNCHEZ¹, ¹Facultad de Ciencias Físico-Matemáticas, Universidad Autónoma de Nuevo León, México, ²Facultad de Ciencias Químicas, Universidad Autónoma de Nuevo León, México

Graphene sheets were formed in water as a result of dispersion and destruction of graphite at room temperature using a water-soluble cobalt octacarboxyphthalocyanine, theraphthal (TP), together with ascorbic acid (AA) in ultrasonic treatment conditions. The goal of this work was to establish the mildest conditions in which the graphite could form graphene or graphene oxide layers in aqueous media without strong reagents (acids). The synthesis was carried out using different amounts of graphite, AA

and TP, which were ultrasonicated in 30 mL flasks with DI water for 5 h in ultrasonic cleaner. The destruction of graphite layers in these conditions does not correspond to the classical concept of π - π stacking interactions and/or σ -bonding between macrocycles and carbon phases. The destruction of graphite forming oxidized graphene (graphene oxide, GO) is explained by free radical processes taking place in the TP-AA aqueous system under strong cavitation conditions only. Characterization of samples was carried out by IR- and Raman spectroscopy, and TEM. Both pristine and COOH-functionalized graphite can be easily solubilized by dispersion in water using highly water-soluble TP in ultrasonic treatment conditions. The final structure depends on the ratio of reagents (graphite-TP-AA). In diluted dispersions, the formation of honeycomb structures was observed, while in relatively concentrated solutions of graphene, the sheets were formed. Results of this research could be applied further to studying low-temperature preparation methods for graphene and other carbon nanostructures.

HARVESTING WASTE HEAT ENERGY USING THERMOELECTRIC GENERATION – INCREASING EFFICIENCY THROUGH ADDITION OF NANO-INCLUSIONS IN THERMOELECTRIC CERAMICS. JAMES PENNEY², XUEYAN SONG¹, CULLEN BOYLE¹, and CESAR-OCTAVIO ROMO-DE-LA-CRUZ¹, ¹Department of Mechanical & Aerospace Engineering, West Virginia University, Morgantown, WV 26505, ²Alan G. MacDiarmid Nanotech Institute, Richardson, TX, 75080

Thermoelectric generation is the process of converting heat directly into electricity through the Seebeck Effect. The Seebeck Effect occurs when two dissimilar conductive materials create a voltage difference from a temperature difference between them. The ability of a material to create a voltage from a temperature difference is measured by the Seebeck Coefficient (S). This can be used to recycle energy from a multitude of areas such as the industrial sector and automobiles. The solution comes from complex metal oxide-based thermoelectrics that are stable in air and at high temperatures. These materials are compared with thermoelectrics made of covalent alloys that have ideal properties but are toxic, costly, and unstable. Choosing materials that are safe and improving their properties are the best options. The efficiency of these materials needs to be improved. They are characterized by their electrical properties, that need to be increased, and thermal properties, that need to be decreased. Doping with gold nano-inclusions will reduce thermal conductivity (k) by increasing phonon scattering while not affecting electrical conductivity ($1/\rho$) or the Seebeck Coefficient. The overall efficiency of the material is measured as Figure of Merit [$ZT=(S^2 * T) / (k * \rho)$]. Samples of an un-doped material, bismuth doped material, and these same materials doped with gold nano-inclusions at different concentrations are

tested for electrical and thermal properties to be compared. Thermoelectrics are of N-type, having excess electrons, and P-type, having a deficiency of electrons, which work together to create the thermoelectric generator. Both materials need to be efficient to create an efficient thermoelectric generator. For this study, the P-type is $\text{Ca}_3\text{Co}_4\text{O}_9$ (CCO) and the N-type is CaMnO_3 (CMO). After the material with the dopant had already been mixed and heated to reaction, the nano-inclusions were created through a hydrothermal process and mixed in with the other material to be pressed and sintered. The nano-inclusions have to be mixed in an un-doped composite of CCO and CMO, which could decrease the concentration of the bismuth dopant. Scanning Electron Microscopy, X-Ray Diffraction, and Electron Dispersive X-Ray Spectroscopy were performed on the samples to determine the location and distribution of the nano-inclusions. Figure 1 shows that the nano-inclusions were found located on the grain boundaries of the composites, evenly distributed. Doped with bismuth, CCO and CMO showed an increase in electrical conductivity and Seebeck coefficient and a decrease in thermal conductivity resulting in minimal change overall. However, the un-doped composites showed noticeable overall improvements in electrical properties at higher temperatures without affecting thermal properties. Contradicting the original design of gold nano-inclusions, the addition of the nano-inclusions slightly improved the electrical properties more than thermal properties. This can be due to the nano-inclusions, small sample size with user error, or due to an overabundance of bismuth dopant in the composites. As the nano-inclusions were added, the concentration of bismuth decreased. This study shows that a small change in the dopant concentration can result in noticeable change in electrical properties.

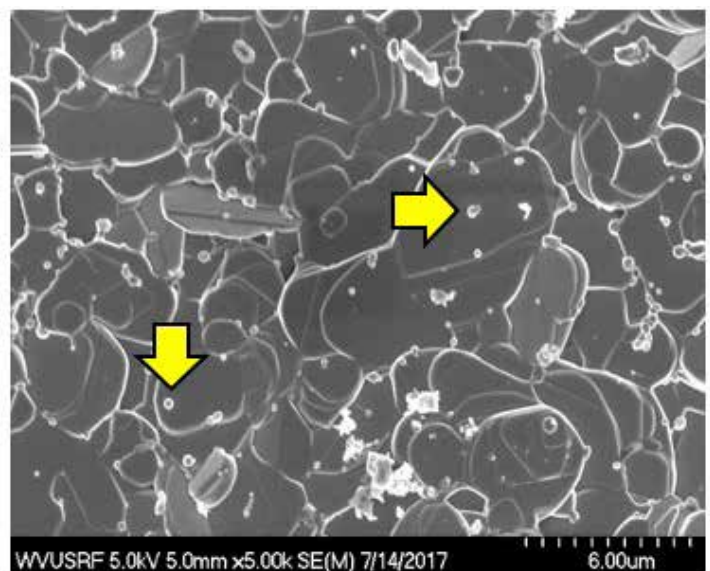


Fig. 1 – Gold nano-inclusions shown in $\text{Ca}_3\text{Co}_4\text{O}_9$ Bismuth at 1.5% Au.

ADVANCED ELECTRON MICROSCOPY OF UNCONVENTIONAL PLASMONIC NANOPARTICLES. SADEGH YAZDI, Department of Materials Science and Nano-Engineering, Rice University, Houston, Texas 77005, United States

Nanoparticles with metallic behaviour that sustain localized surface plasmon resonances (LSPRs) are of great interest in diverse fields ranging from medicine to optoelectronics to photocatalysis. Ag and Au nanoparticles are commonly used in plasmonic devices as building blocks. These precious metals are rare, with resonances limited in the visible range. In search for new plasmonic nanoparticles, a wide range of materials including earth abundant metals, semiconductors, conducting oxides, 2D materials, and topological insulators have been studied in recent years. In understanding the structural, compositional, electrical and optical properties of these materials, transmission electron microscopy plays a critical role. Figure 1 shows representative results of our recent electron microscopy studies on four different plasmonic nanostructures: Al nanoparticles decorated with different transition metals, colloiddally synthesized hexagonal Mg nanoplates, F and Sn doped indium oxide nanocubes, and hydrothermally grown hexagonal Bi_2Te_3 nanoplates. In each case, analyses were carried out on individual nanoparticles using atomic resolution HAADF-STEM, monochromated STEM-EELS, and STEM-EDS.

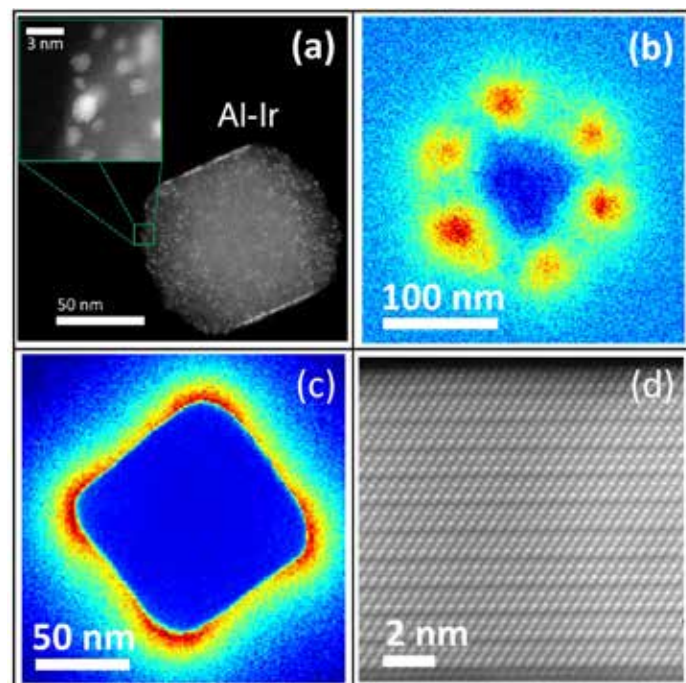


Fig. 1. Representative examples of advanced electron microscopy of unconventional plasmonic nanoparticles. (a) HAADF-STEM image of Al nanoparticle decorated with Ir; Monochromated EELS plasmon map of corner mode (b) in a hexagonal Mg nanoplate and (c) in an F and Sn doped indium oxide nanocube; (d) A cross sectional atomic resolution HAADF-STEM image of hexagonal Bi_2Te_3 nanoplate.

POROUS SILICON OXYCARBIDE (SiCO) MATERIALS. SUSANA AGUIRRE-MEDEL, PETER KROLL*, Chemistry and Biochemistry Department, University of Texas at Arlington

We report the synthesis of porous silicon oxycarbide (SiCO) materials, their microstructural characterization and performance in environmental applications. One of the synthesis processes consisted of reacting siloxane precursors containing Si-H bonds with cross-linkers bearing vinyl groups using a platinum catalyst. The reaction in diluted solutions (80-95%) converted the siloxanes into aerogels after supercritical drying in CO_2 . This yielded a porous material ranging from 100 to 400 m^2/g of BET SSA, depending on the solvent of synthesis. The other synthesis method involved hydrolysis and condensation reactions to obtain a cross-linked gel which was slowly dried at 45°C to obtain a porous material with up to 800 m^2/g of BET SSA, as obtained from N_2 adsorption measurements. Porous SiCO materials were transformed *via* thermal treatment in controlled atmospheres into SiCO ceramics. We characterized the specific surface area of porous SiCO materials, nanoparticle size, pore size distribution, average pore size, and total porosity using SEM and TEM imaging. Porous SiCO materials displayed high adsorption percent of methylene blue (75%) and methyl violet (49%) solutions in less than 5 minutes of reaction. These materials have potential applications for environmental remediation.

TECHNICAL ABSTRACTS Spring 2018

ELECTRON HOLOGRAPHY AND DETERMINATION OF BEST ACQUISITION CONDITIONS. ARTURO PONCE¹, EDUARDO ORTEGA¹, SANDRA VERGARA^{1*}, and EDGAR VOELKL², ¹Department of Physics and Astronomy, University of Texas at San Antonio, One UTSA Circle, San Antonio, TX 78249, ²HoloWerk LLC, Germantown, MD 20876

Investigation of magnetic, electric and beam sensitive samples significantly benefits from the use of electron holography (EH). The benefit is given via access to information beyond the standard image intensity, referred to as the image phase (Ortega *et al.*, *AIP Advances* 8, 2018). Current approaches for gaining access to the image phase include variations of the Zernike phase contrast or differential phase contrast. So far, EH provides the most direct and reliable access to the image phase but its requirements are strict and the coherence of the electron source remains a significant limitation. Therefore, it is important to set up the microscope and the acquisition system such as to provide the best possible phase image data.

We have been using our Cs corrected JEOL ARM 200F

microscope operated at 200 keV for acquiring holograms that deliver a high signal/noise ratio in the image phase. For this we predict, live and in real time, the quality of holograms as a function of exposure time (t_{exp}) and condenser setting. An example of hologram quality as a function of t_{exp} for constant illumination is given in Fig. 1. In literature, interference fringe contrast is often referred as the key parameter for hologram quality. However, a hologram with 100% fringe contrast μ but no electrons is just as bad as a hologram with infinite number of electrons ($N \rightarrow \infty$) and $\mu = 0\%$. The optimum fringe contrast is proportional to the expression for hologram quality $Q \sim \mu \sqrt{N}$, defined by the brightness of the electron gun. Another parameter needing consideration is the drift of the interference fringes over time, considered as an upper limit to t_{exp} . Less known is the detail that there also is a lower exposure time limitation due to the beam blanker of the microscope (Voelkl and Tang, *Ultramicroscopy* 110, 2010), typically, as the beam returns from its deflection and slows until it comes to rest. That delay time frame with the illumination in movement is critical for EH as the biprism is far out of focus and thus strongly affected by beam movements. Therefore, it is important to track all these parameters in a simple, straightforward manner shown in Fig. 1. The teal colored and filled line plot tracks the interference fringe contrast, while the green line plot tracks the hologram quality (proportional to the standard deviation in the phase image). The track for the fringe drift is suppressed here. The exposure time t_{exp} starts on the left at 0.125s, increases to 4s and returns to 0.125s in steps of a factor multiple of 2. The Q-factor therefore should change in increments of $\sqrt{2}$, i.e. in decreasing order: [14.8, 10.5, 7.4, 5.3, 3.7, 2.6, 1.85], whereas the measured values are [14.8, 10.2, 6.6, 3.8, 2.4, 1.4] indicating a significant drop below the expected values for Q due to the shutter speed of the deflectors above the sample.

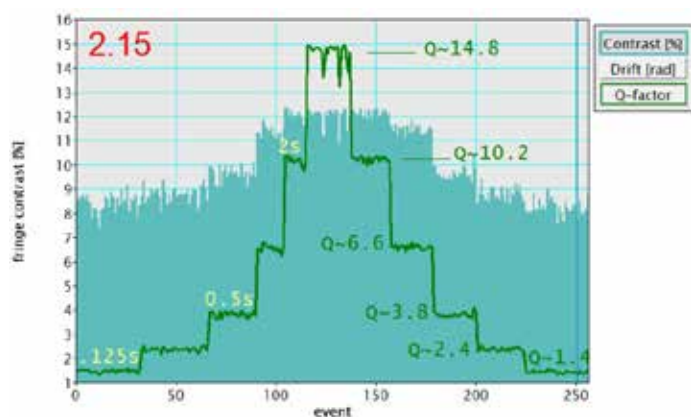


Fig. 1. – Hologram quality Q and fringe contrast μ as a function of t_{exp} ranging from 0.125s to 4s and back to 0.125s. As discussed in the text, short exposure times, less than 1s, affect the hologram quality negatively.

As a result of these measurements, it appears that exposure times for holographic imaging should be in the range of 1–4s exposure time in the microscope used. Consecutive single holograms are registered in image stacks yielding high phase sensitivity on a regular basis. Examples of holographic imaging of magnetic fields will be shown demonstrating the routinely achievable high quality of holographic data on the JEOL ARM 200F microscope.

TEACHING METHODOLOGY ABSTRACTS Spring 2018

ENGAGING PRE-SERVICE TEACHERS IN USING THE ZPIX 300 ZOOM DIGITAL MICROSCOPE FOR STATE STANDARDS-ALIGNED SCIENCE LESSONS.
SANDRA MUHITCH and SANDRA WESTMORELAND,
Texas Woman's University, Department of Biology, Denton, Texas

This project was designed to determine the feasibility of using the zPIX 300 Zoom Digital Microscope for teaching an inquiry science lesson about the life cycle of insects to pre-service teachers. This lesson was intended for a fifth grade science class and was aligned with the Texas Essential Knowledge and Skills (TEKS), which are part of the required curriculum for Texas public schools. At the conclusion of the lesson, students were expected to be able to ask well-defined questions and to use appropriate equipment and technology to describe the differences between insect complete and incomplete metamorphoses. A culture of rice weevils which contained live samples of the different metamorphic stages was presented to the class. Students viewed the samples using the hand-held digital microscope and identified the three stages of insect development by comparing them to manipulative models and pictures of other insect life cycles. Students were able to successfully identify and document the metamorphic stages of the rice weevil, including the larvae within grains of rice, the pupa, and the adult. Students stated that using the digital microscope made the lesson more engaging and promoted inquiry as they “discovered” the stages of metamorphosis in their samples. In addition, they commented that the tool was easy to set up and use and could easily be incorporated in future lessons. Pre-service teachers participating in the lesson were asked to comment on the effectiveness of the microscope use in this lesson. One feature that the pre-service teachers noted was the ability to capture digital photos and videos for documenting students' investigations. The zPIX Zoom Digital Microscope is a valuable tool for teaching science concepts in the classroom. It gives younger students the opportunity to use a microscope for the first time, while enhancing inquiry learning experience and the use of technology. This affordable tool could be adapted to teach a wide range of science concepts.

JOIN TEXAS SOCIETY FOR MICROSCOPY ON FACEBOOK

TSM
e⁻

Texas Society for Microscopy
Non-Profit Organization

Like Follow Message

Timeline About Photos Likes More

68 people like this

Invite friends to like this Page

ABOUT

TSM Mission Statement: The purpose of this Society is to further the use, understanding, and knowledge of all aspects of microscopy and their applications...

READ MORE

<http://www.texasmicroscopy.org/index.html>

Post Photo / Video

Write something...

Post

Texas Society for Microscopy added 117 new photos to the album: 50th Meeting of the Texas Society for Microscopy 2015 — at UT Austin. March 9

Texas Society for Microscopy 2015

CALL FOR PAPERS

Authors are invited to submit their manuscripts for the next edition of the Texas Journal of Microscopy. The objective of the journal is to publish papers on original research and developing methods for providing prospect guidelines to research supported by all forms of microscopy. Please send your work as short communications, full articles or review articles in biological sciences, material sciences or education to either journal editor:

Camelia Maier
cmaier@twu.edu

Catalina I. Pislariu
cpislariu@twu.edu

BEAM DECELERATION IMPROVES IMAGE QUALITY OF BUTTERFLY WING SCALES IN THE SCANNING ELECTRON MICROSCOPE

BERND ZECHMANN

Baylor University, Center for Microscopy and Imaging, One Bear Place #97046
Waco, Texas 76798, Bernd_Zechmann@baylor.edu

Abstract

Beam deceleration has become a commonly used tool in scanning electron microscopy for imaging material samples. By applying a negative bias voltage on the sample, or the whole stage, the landing energy of the beam is reduced, which in turn reduces charging effects and related image distortions. The aim of this study was to compare the image quality of butterfly wings at high and low vacuum conditions, with and without beam deceleration in the scanning electron microscope (SEM). The effects of charging on the sample resulted in shifted line scans, distorted ultrastructure, and fuzzy edges. Charged edges were commonly observed when the scales of the butterfly wings were imaged at 5 kV and 3 kV under high vacuum conditions. Under low vacuum conditions, charging effects were almost completely neutralized. Signal strength, however, was greatly reduced resulting in grainy image quality and loss of detail to the fine structures of the butterfly wings. Likewise, beam deceleration at high vacuum condition eliminated charging effects leading to superior image quality. Even at high magnification fine structures of butterfly wings were clearly visible without image distortions. In conclusion, imaging butterfly wings with beam deceleration resulted in superior image quality when compared to images obtained without beam deceleration at high and low vacuum conditions.

Keywords: beam deceleration, butterfly wing, low vacuum, SEM

Introduction

The charging of a sample is a commonly observed artifact when samples with low conductivity are imaged in the SEM (Cazaux, 2004; Kim *et al.*, 2010; Sim *et al.*, 2010; Flatabø *et al.*, 2017). In order to avoid such artifacts, non-conductive samples are often coated with a fine layer of conductive metal, e.g. gold, iridium, palladium, or carbon, so that the electrons from the beam can flow off. If not carefully applied, they obscure structures of interest or build new structures on the surface of the sample (Stokross *et al.*, 1998; Golding *et al.*, 2016). Alternatively, non-conductive samples can be observed in low vacuum/variable pressure conditions where charging effects are neutralized by ionized residual gas molecules in the specimen chamber (James, 2009; Miyazaki *et al.*, 2012). This technique enables even the observation of wet biological samples without coating them with a conductive layer of metal or carbon (Miyazaki *et al.*, 2012).

Another approach in imaging samples with low conductivity is the application of beam deceleration (Phifer *et al.*, 2009). The principle behind beam deceleration is that the specimen or whole stage is held at a negative bias voltage. Electrons that leave the final lens are decelerated by this negative bias voltage before they reach the specimen (Phifer *et al.*, 2009). Landing energy describes the energy of the beam that interacts with the sample and is determined by the initial voltage of the beam minus the stage bias voltage. Even though beam deceleration has been extensively tested on material samples such as copper/palladium solder alloy, silica, nanomaterial, such as tin on carbon, diamond, gold (Phifer *et al.*, 2009; Miyazaki *et al.*, 2012) and polymers (Wan *et al.*, 2016), very little information has been available on how this technique advances imaging capabilities of biological samples in the SEM. Recently, it has been reported that beam deceleration improves imaging of biological samples embedded in plastic resin (Ohta

et al., 2012), but reports on the beam deceleration effects on biological material is non-existent. In order to study the effects of beam deceleration on imaging quality of biological samples in the SEM, this work compared the ultrastructure of butterfly wings observed under low and high vacuum conditions, with and without beam deceleration.

Materials and Methods

Pieces of a butterfly wing (Gulf Fritillary, *Agraulis* sp.) were air dried and mounted on aluminum stubs with carbon tape. Some samples were sputter coated with a 15 nm layer of iridium, while other samples were imaged without coating. Coated and uncoated samples were observed with a Versa 3D SEM (FEI, OR, USA) at: a) high vacuum mode (approximately 5×10^{-6} mbar) at 5 kV; b) high vacuum mode (approximately 5×10^{-6} mbar) at 3 kV; c) low vacuum mode (1.3 mbar) at 30 kV; and d) at high vacuum mode (approximately 5×10^{-6} mbar) at 5 kV with beam deceleration. When beam deceleration was used, high voltage was set to -5 kV and the stage bias was set to -2 kV. Thus, the electrons in the column were accelerated to 5 kV and then decelerated by 2 kV before they reached the sample with 3 kV. Therefore, the primary electrons that reached the sample had an energy of 3 kV when beam deceleration was used. All images were taken at a working distance of 10 mm, with a spot size of 5, a dwell time of 30 μ s, and a resolution of 1536 x 1024 pixels.

Results and Discussion

Charging was commonly observed on the surface of butterfly wings when they were imaged at high and low vacuum conditions without beam deceleration at 3 kV, 5 kV and 30 kV (arrows in Figs. 1 A-C and 2 A-C). Even though charging did not significantly obstruct image quality at low magnification

(Fig. 1 A-C), it significantly decreased image quality at higher magnification resulting in shifted line scans, distorted ultrastructure, and charged edges (Fig. 2 A and B). Under these conditions, coating the samples with a conductive layer of metal should have prevented the charging effects (Flatabø *et al.*, 2004). Nevertheless, in this study sputter coating butterfly wings with 15 nm of iridium proved to be inefficient at preventing charging and artifacts deriving from it (Fig. 2 A and B). Imaging uncoated butterfly wing samples at low vacuum conditions also proved to be ineffective. Under low vacuum conditions, charging effects were almost completely neutralized by ionized residual gas molecules in the specimen chamber (James, 2009; Miyazaki *et al.*, 2012). However, the signal to noise ratio was very low under these conditions resulting in grainy image quality and low resolution made it difficult to image fine structural details of the butterfly wing scales at high magnification (Figs. 1 C and 2 C).

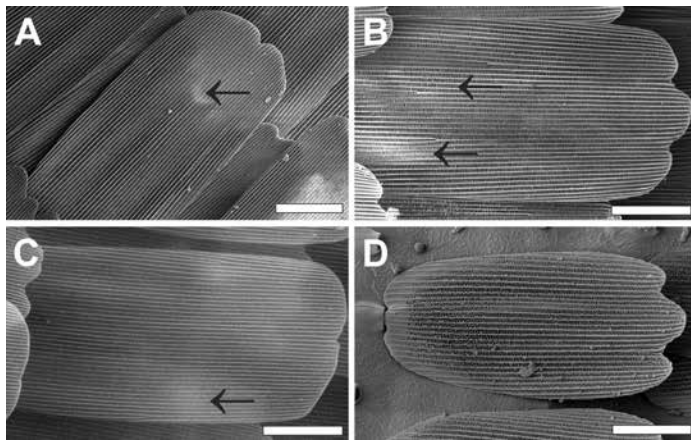


Fig. 1. SEM micrographs of a butterfly wing scale taken at different kV and vacuum mode settings: A) high vacuum mode at 5 kV, B) high vacuum mode at 3 kV, C) low vacuum mode at 30 kV, and D) high vacuum with 5 kV beam acceleration, 2 kV beam deceleration and a final beam energy on the surface of the sample of 3 kV. Arrows show image distortions due to charging. Bars = 30 μm .

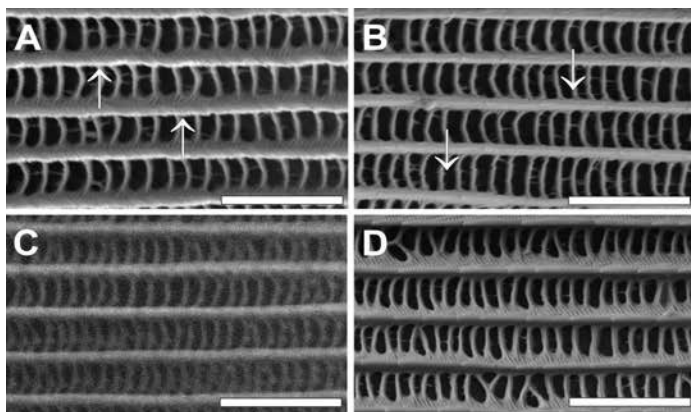


Fig. 2. Close up of a butterfly wing scale taken at different kV and vacuum mode settings: A) high vacuum mode at 5 kV, B) high vacuum mode at 3 kV, C) low vacuum mode at 30 kV, and D) high vacuum with 5 kV beam acceleration, 2 kV beam deceleration and a final beam energy on the surface of the sample of 3 kV. Arrows show image distortions such as charging, blurry edges, and shifted structures. Bars = 5 μm .

Imaging the scale of the butterfly wing under high vacuum conditions with beam deceleration yielded superior image quality (Figs. 1 D and 2 D). Charging was not observed under these conditions and fine structural details on the scales of the butterfly wing were clearly visible even at high magnifications (Figure 2 D). The application of beam deceleration and its advantages for imaging samples with low conductivity already have been widely recognized for material samples (Phifer *et al.*, 2009; Miyazaki *et al.*, 2012; Wan *et al.*, 2016) as well as for biological samples embedded in plastic resin (Ohta *et al.*, 2012). This study extends these observations and demonstrates that beam deceleration leads to superior image quality of un-embedded biological specimens. In conclusion, beam deceleration at high vacuum conditions proved to be the most efficient method to image butterfly wings in the SEM. Charging artifacts, commonly observed at low and high vacuum conditions without beam acceleration, were reduced to a minimum when beam deceleration was used resulting in superior image quality even at high magnification.

References

- Cazaux, J. 2004. Charging in scanning electron microscopy “from inside and outside”. *Scanning* 26:181-203.
- Flatabø, R., Coste, A., and Greve, M.M. 2017. A systematic investigation of the charging effect in scanning electron microscopy for metal nanostructures on insulating substrates. *Journal of Microscopy* 265:287-297.
- Golding, C.G., Lamboo, L.L., Beniac, D.R., and Booth, T.F. 2016. The scanning electron microscope in microbiology and diagnosis of infectious disease. *Scientific Reports* 6: 26516, DOI: 10.1038/srep26516.
- James, B. 2009. Advances in “wet” electron microscopy techniques and their application to the study of food structure. *Trends in Food Science and Technology* 20:114-124.
- Kim, K.H., Akase, Z., Suzuki, T., and Shindo, D. 2010. Charging effects on SEM/SIM contrast of metal/insulator system in various metallic coating conditions. *Materials Transactions* 51:1080-1083.
- Phifer, D., Tuma, L., Vystavel, T., Wandrol, P., and Young, R.J. 2009. Improving SEM imaging performance using beam deceleration. *Microscopy Today* 17:40-49.
- Miyazaki, H., Uosaki, H., Tojo, A., Hirashima, S., Inaga, S., Sakuma, K., Morishita, Y., and Fukayama, M. 2012. Application of low-vacuum scanning electron microscopy for renal biopsy specimens. *Pathology-Research and Practice* 208:503-509.
- Ohta, K., Sadayama, S., Togo, A., Higashi, R., Tanoue, R., and Nakamura, K. 2012. Beam deceleration for block-face scanning electron microscopy of embedded biological tissue. *Micron* 43:612-620.
- Sim, K.S., Tan, Y.Y., Lai, M.A., Tso, C.P., and Lim, W.K. 2010. Reducing scanning electron microscope charging by using exponential contrast stretching technique on post-processing images. *Journal of Microscopy* 238:44-56.
- Stokroos, I., Kalicharan, D., Van der Want, J.J.L., and Jongebloed, W.L. 1998. A comparative study of thin coatings of Au/Pd, Pt and Cr produced by magnetron sputtering for FE-SEM. *Journal of Microscopy* 189:79-89.
- Wan, Q., Masters, R.C., Lidzey, D., Abrams, K.J., Dapor, M., Plenderleith, R.A., Rimmer, S., Claeysens, F., and Rodenburg, C. 2016. Angle selective backscattered electron contrast in the low-voltage scanning electron microscope: Simulation and experiment for polymers. *Ultramicroscopy* 171:126-138.



Advanced Multi Application Autosamdri®-931

- ✓ NEW ! Post Process Data Review Feature
- ✓ Patent Pending “Stasis Software” for Challenging Samples
- ✓ Touchscreen Control Critical Point Dryer
- ✓ Automatic & Custom Programmable Recipes
- ✓ Available in Three Chamber Sizes
- ✓ Cleanroom System Option
- ✓ Made in U.S.A.

Corporate Members



AMETEK (EDAX, Inc.)

www.ametek.com
John Haritos
392 East 12300 South, Suite H
Draper, UT 84020
201-466-0907
John.Haritos@ametek.com

BioTek Instruments, Inc.

www.biotek.com
Vanessa Meyer
100 Tigan Street
Winooski, VT 05404
847-757-3387 meyv@BioTek.com

Bruker AXS, Inc.

www.bruker.com
John Mastovich
3194 Beverly Court
Murrysville, PA 15668
908-419-8225
Austin, TX 78747
john.mastovich@bruker.com

CARL ZEISS SMT

www.zeiss.com/nts
Laura Grafflin
One Corporation Way
Peabody, MA 01960
978-826-1500 978-532-5696 Fax
laura.grafflin@zeiss.com

Electron Microscopy Science/Diatome

www.emsdiasum.com/microscopy/
Robert Armstrong
1560 Industry Road, P.O. BOX 550
Hatfield, PA 19440
800-523-5874 215-412-8450 Fax
rarmstrong@emsdiasum.com

E.A. Fischione Instruments, Inc.

www.fischione.com
Nicole Dengler
9003 Corporate Circle
Export, PA 15632
724-325-5444
nm_dengler@fischione.com

Gatan, Inc.

www.gatan.com
James Long
5794 W. Las Postias Blvd.
Pleasanton, CA 94588
512-657-0898 925-463-0504 FAX
JLong@gatan.com

Hitachi High Technologies America

www.hitachi-hta.com
Rod Baird
1375 North 28th Ave., PO Box 612208
Irving TX 75261
214-537-2158 972-615-9300 Fax
rod.baird@hitachi-hta.com

IXRF Systems

www.ixrfsystems.com
Dave Bush
10421 Old Manchaca Rd., Suite 620
Austin, TX 78748
512-386-6100 512-386-6105 Fax
daveb@ixrfsystems.com

JEOL USA, Inc.

www.jeolusa.com
Zane Marek
13810 Paisano Circle
Austin, TX 78737
978-495-2176 marek@jeol.com

Leica Microsystems, Inc.

www.leica-microsystems.com
Andrew Robertson
1700 Leider Lane
Buffalo Grove, IL 60089
209-603-6874 847-607-7024 FAX
Andrew.Robertson@leica-microsystems.com

M.E. Taylor Engineering, Inc.

www.semsupplies.com
SEMico Division
15817 Crabbs Branch Way
Rockville, MD 20855
301-975-9798 sales@semicro.org

Micro Star Technologies, Inc.

www.microstartech.com
Cathy Ryan
511 FM 3179
Huntsville, TX 77340
936-291-6891 or 800-533-2509
cathy.ryan@microstartech.com

Nikon Instruments Inc.

www.nikoninstruments.com
Clay Williams
1300 Walt Whitman Road
Melville, NY 11747-3064
972-693-7779 swilliams@nikon.net

Oxford Instruments America, Inc.

www.oxford-instruments.com
David Richards
300 Baker Avenue, Suite 150
Concord, MA 01742
978-369-9933 x 201
david.richards@oxinst.com

Protochips

www.protochips.com
Robert Monteverde
3800 Gateway Centre Blvd., Suite 306
Morrisville, NC 27560
919-377-0800
Robert.Monteverde@protochips.com

Rigaku

www.rigaku.com
Michelle Goodwin
9009 New Trails Dr.
The Woodlands, TX 77381
281-362-2300 ext. 122
Michelle.Goodwin@rigaku.com

RMC Boeckeler

www.rmcbocckeler.com
Erin Jordan
4650 Butterfield Drive
Tucson, AZ 85714
520-745-0001 520-745-0004 Fax
erin@boeckeler.com

Scientific Instrumentation Services

www.scientificinstrumentationservices.com
Alexander Green
1125A Regal Row
Austin, TX, 78748
512-520-4940
contact@electronmicroscoperepair.com

Ted Pella, Inc.

www.tedpella.com
David Rollings
PO Box 462477
Redding, CA 96049-2477
530-243-2200 or 800-237-3526
sales@tedpella.com

TESCAN USA, Inc

www.tescan-usa.com
Mike Craig
765 Commonwealth Drive, Suite 101
Warrendale, PA 15086
512-417-8990 Mike.Craig@Tescan-USA.com

Thermo Fisher Scientific

www.thermofisher.com
www.fei.com
Michael Howren
Life Science - Light Microscopy
281-614-9916
mike.howren@thermofisher.com
Tony Carpenter
Life Sciences - Electron Microscopy
480-650-8190
tony.carpenter@thermofisher.com
Dan Gostovic
Materials Science - Electron Microscopy
dan.gostovic@thermofisher.com

Tousimis

www.tousimis.com
Yianni Tousimis
2211 Lewis Avenue
Rockville, MD 20851
301-881-2450 301-881-5374 Fax
ytousimis@tousimis.com

VISIT TSM WEBSITE

Visit us at [http:// www.texasmicroscopy.org](http://www.texasmicroscopy.org) to take a look at important features such as membership, meetings, journal issues, small grant program and more!

**TEXAS SOCIETY FOR MICROSCOPY**
"Embracing All Forms of Microscopy"

[HOME](#) | [ABOUT US](#) | [MEMBERSHIP](#) | [MEETINGS](#) | [JOURNALS](#) | [SMALL GRANT](#) | [LINKS](#)



**** Next TSM Meeting ****
February 22 - 24, 2018
[Register Here!](#)
Hilton Garden Inn
Danton

TSM Annual Meeting in Denton
February 22-24, 2018
[Click Here for Registration](#)
[Click Here for Final Program and Further Details](#)

The Texas Society for Microscopy (TSM) was founded in 1963 and has become an informative resource for many scientists since then. We welcome microscopists, researchers, students and administrators from all disciplines and backgrounds who are interested in microscopy or the science of microscopy.

Our non-profit organization is committed to advancing knowledge and understanding of all aspects of microscopy and their applications as they apply to life sciences, materials sciences and industry. We are committed to support students through our [Small Grant Program](#) and through travel grants to attend our annual meetings. The society is also represented at the meetings of the Microscopy Society of America through our president. The [annual meetings](#) of the TSM are a highlight for our members and enjoy wide corporate support.

We invite you to become a member of the TSM and support its mission and vision through your [membership](#).



join us on
facebook
[TSM is on Facebook!](#)



MSA
Microscopy Society of America



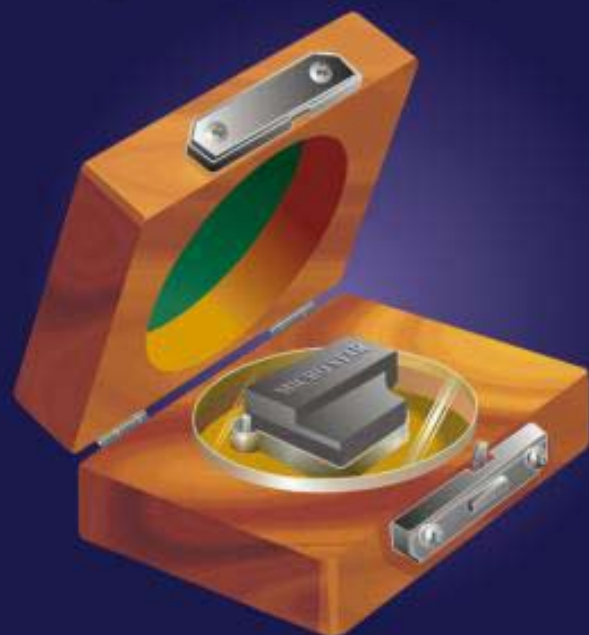
© 2017 Texas Society for Microscopy

MICRO STAR DIAMOND KNIFE

TYPES

TYPES	AVAILABLE EDGE LENGTHS	AVAILABLE INCL. ANGLES*	RANGE OF SECTION THICKNESS	APPLICATIONS
SU	1 to 8 mm	45° 35° 55°	25nm to 200nm	Standard ultramicrotomy sectioning of biological and other material specimens.
CW	1 to 8 mm	45° 35°	50nm to 1 μ m	Frozen specimens sectioned wet with liquids like ethylene glycol. Set in "W" style boat.
CD	1 to 8 mm	45° 35°	50nm to 1 μ m	Frozen specimens sectioned dry. Set in "D" style boat.
TS	1 to 8 mm	45° 55°	50nm to 2 μ m	Thick sections or alternating thick and thin sections.
MT	2 to 8 mm	45° 55°	50nm to 2 μ m	Industrial materials sectioning. Not tested to the same ultra high standards as the types above, hence their lower price.
LC	4 to 12 mm	45° 55°	0.1 μ m to 5 μ m	Frozen specimens to be examined at light microscopy magnifications. Set in "D" or "W" style boat.
LH	4 to 12 mm	45° 55°	0.1 μ m to 5 μ m	Sections to be examined at light microscopy magnifications.

* The standard included angle of 45° is suitable for most applications. Knives with 35° reduce morphological deformation but the edge is more fragile. 55° is recommended for routine hard specimen sectioning. Custom angles and lengths available per request at no extra cost.



MICRO STAR diamond knives are manufactured exclusively from the purest quality natural diamonds, using the most advanced technologies. Our quality inspection laboratory includes two TEM one SEM and one Atomic Force Microscope.

MICRO STAR is the only diamond knife whose unsurpassed quality is backed by one year guarantee, and two month testing period before payment.

Every MICRO STAR diamond knife is packaged in a precision hand crafted wood case for life time shipping and storage protection.

Per request, you may get your resharpened knife set in a new MICRO STAR boat and box at no extra cost.

MICRO STAR TECHNOLOGIES
511 FM 3179 RD
HUNTSVILLE, TX 77340
936-291-6891

EMS has it!

A comprehensive selection of the finest hand-made tweezers for every research requirement, including...

- Medical Tweezers
- High Precisions and Ultra Fine Tweezers
- Thin and Long
- Ergonomic
- Flat Tip
- Ceramic and Ceramic Tipped
- ESD Safe
- General Purpose Tweezers
- Fiber and Fiber Tipped
- EMS Synthetic Fiber Tweezers
- Surface Mount and Optoelectric
- Wafer

and our newest additions:

EMS Gold Coated Tweezers

Finely crafted, high precision tweezers made from anti-acidic, non-magnetic stainless steel, plated with 2 microns of pure 24-carat gold.



EMS High Precision, Diamond Like Carbon (DLC) Tweezers

Feature tips covered in a pure diamond film grown directly on the exposed metallic substrate via an innovative plasma-assisted deposition technique.



now also available in medical grade...

EMS Tweezers

NEW EMS High End Medical Tweezers

EMS is proud to introduce this new category of tweezers. They are all handcrafted to perfect tip symmetry and balance and the surface has an electropolish finish. With high precision fine tips and dot-serrated handles for a perfect grip. All of these tweezers can be sterilized and they are all made from Inox.



EMS is proud to provide a full selection of tweezers and forceps with all hand-crafted to a perfect tip symmetry and balance, high quality and innovative tweezers, that are well suited for many applications:

- EM Labs • General Labs • Electronic • Aerospace • Precision Assembly • Optics • Biotech • Chemistry • Surgery • and more**

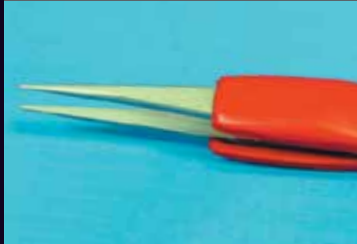
CONTACT US FOR MORE INFORMATION...

**Electron
Microscopy
Sciences**

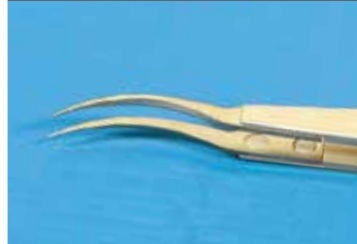
P.O. Box 550 • 1560 Industry Rd.
Hatfield, Pa 19440
Tel: (215) 412-8400
Fax: (215) 412-8450
email: sgkcck@aol.com
or stacie@ems-secure.com

www.emsdiasum.com

ESD SAFE
TWEEZERS



ERGONOMIC
TWEEZERS



SUPER SLIM
TWEEZERS



FLAT TIP
TWEEZERS



CERAMIC TIP
TWEEZERS



WAFER
TWEEZERS

